






Article

Optimization of Laser-Based Method to Conduct Skin Ablation in Zebrafish and Development of Deep Learning-Based Method for Skin Wound-Size Measurement

Petrus Siregar^{1,2,†}, Yi-Shan Liu^{3,4,5,†} , Franelyne P. Casuga⁶, Ching-Yu Huang⁷, Kelvin H.-C. Chen⁸ , Jong-Chin Huang⁸ , Chih-Hsin Hung⁹, Yih-Kai Lin^{10,*} , Chung-Der Hsiao^{1,2,11,12,*}  and Hung-Yu Lin^{7,13,*}

- ¹ Department of Chemistry, Chung Yuan Christian University, Taoyuan City 320314, Taiwan; siregar.petrus27@gmail.com
- ² Department of Bioscience Technology, Chung Yuan Christian University, Taoyuan City 320314, Taiwan
- ³ Department of Pharmacy, Tajen University, Pingtung 907101, Taiwan; drjulialiu@yahoo.com.tw
- ⁴ Department of Dermatology, E-Da Hospital, I-Shou University, Kaohsiung 84001, Taiwan
- ⁵ School of Chinese Medicine for Post Baccalaureate, College of Medicine, I-Shou University, Kaohsiung 84001, Taiwan
- ⁶ Department of Pharmacy, Research Center for the Natural and Applied Science, University of Santo Tomas, Manila 1008, Philippines; fpcasuga@ust.edu.ph
- ⁷ Division of Urology, Department of Surgery, E-Da Dachang Hospital, Kaohsiung 80794, Taiwan; ed102747@edah.org.tw
- ⁸ Department of Applied Chemistry, National Pingtung University, Pingtung 90003, Taiwan; kelvin@mail.nptu.edu.tw (K.H.-C.C.); hjc@mail.nptu.edu.tw (J.-C.H.)
- ⁹ Institute of Biotechnology and Chemical Engineering, I-Shou University, Kaohsiung 84001, Taiwan; chhung@isu.edu.tw
- ¹⁰ Department of Computer Science, National Pingtung University, Pingtung 90003, Taiwan
- ¹¹ Center for Nanotechnology, Chung Yuan Christian University, Taoyuan City 320314, Taiwan
- ¹² Research Center for Aquatic Toxicology and Pharmacology, Chung Yuan Christian University, Taoyuan City 320314, Taiwan
- ¹³ School of Medicine, College of Medicine, I-Shou University, Kaohsiung 84001, Taiwan
- * Correspondence: yklin@mail.nptu.edu.tw (Y.-K.L.); cdhsiao@cycu.edu.tw (C.-D.H.); ed100464@edah.org.tw (H.-Y.L.)
- † These authors contributed equally to this work.



Citation: Siregar, P.; Liu, Y.-S.; Casuga, F.P.; Huang, C.-Y.; Chen, K.H.-C.; Huang, J.-C.; Hung, C.-H.; Lin, Y.-K.; Hsiao, C.-D.; Lin, H.-Y. Optimization of Laser-Based Method to Conduct Skin Ablation in Zebrafish and Development of Deep Learning-Based Method for Skin Wound-Size Measurement. *Inventions* **2024**, *9*, 25. <https://doi.org/10.3390/inventions9020025>

Academic Editors: Anastasios Doulamis and Chun-Liang Lin

Received: 20 December 2023

Revised: 9 February 2024

Accepted: 19 February 2024

Published: 27 February 2024



Copyright: © 2024 by the authors. Licensee MDPI, Basel, Switzerland. This article is an open access article distributed under the terms and conditions of the Creative Commons Attribution (CC BY) license (<https://creativecommons.org/licenses/by/4.0/>).

Abstract: Skin plays an important role as a defense mechanism against environmental pathogens in organisms such as humans or animals. Once the skin integrity is disturbed by a wound, pathogens can penetrate easily into a deeper part of the body to induce disease. By this means, it is important for the skin to regenerate quickly upon injury to regain its protective barrier function. Traditionally, scientists use rodents or mammals as experimental animals to study skin wound healing. However, due to concerns about animal welfare and increasing costs of laboratory animals, such as rodents, scientists have considered alternative methods of implementing replace, reduce, and refine (3Rs) in experimentation. Moreover, several previous studies on skin wound healing in fish used relatively expensive medical-grade lasers with a low calculation efficiency of the wound area, which led to human judgment errors. Thus, this study aimed to develop a new alternative model for skin wound healing by utilizing zebrafish together with a new rapid and efficient method as an alternative in investigating skin wound healing. First, in order to fulfill the 3Rs concept, the pain in the tested zebrafish was evaluated by using a 3D locomotion assay. Afterward, the obtained behavior data were analyzed using the Kruskal–Wallis test, followed by Dunn’s multiple comparisons tests; later, 3 watts was chosen as the power for the laser, since the wound caused by the laser at this power did not significantly alter zebrafish swimming behaviors. Furthermore, we also optimized the experimental conditions of zebrafish skin wound healing using a laser engraving machine, which can create skin wounds with a high reproducibility in size and depth. The wound closure of the tested zebrafish was then analyzed by using a two-way ANOVA, and presented in 25%, 50%, and 75% of wound-closure percentages. After imparting wounds to the skin of the zebrafish, wound images were collected and used for deep-learning training by convolutional neural networks (CNNs), either the Mask-RCNN or U-Net, so that the computer could calculate the area of the skin wounds in an automatic manner.

Using ImageJ manual counting as a gold standard, we found that the U-Net performance was better than the Mask RCNN for zebrafish skin wound judgment. For proof-of-concept validation, a U-Net trained model was applied to study and determine the effect of different temperatures and the administration of antioxidants on the skin wound-healing kinetics. Results showed a significant positive correlation between the speed of wound closure and the exposure to different temperatures and administration of antioxidants. Taken together, the laser-based skin ablation and deep learning-based wound-size measurement methods reported in this study provide a faster, reliable, and reduced suffering protocol to conduct skin wound healing in zebrafish for the first time.

Keywords: skin; wound healing; zebrafish; medicine; laser ablation; deep learning; ImageJ

1. Introduction

Skin is known as the body's largest organ in vertebrates and it is a vital organ for protection, defense mechanisms, and survival. It functions as the fundamental mechanical defense from external factors, such as pathogenic microbe invasion and various environmental hazards. Furthermore, the skin maintains body homeostasis through the prevention of excessive water loss and through temperature regulation [1]. Skin can lose its integrity when injured, which consequently results in functional imbalance [2]. Following the injury, the skin regenerates immediately to resume its normal protective shield and barrier function. To survive from wound injury, a multistep mechanism was initiated to prevent further damage and subsequently induce regeneration in the wound-healing area. This biological regeneration process includes a complex cascading reaction of sequential events that are needed by an organism to reach tissue homeostasis [3]. Injured skin will initiate a complex process of events that involves inflammation as well as the formation and restoration of new tissue, which require the regulation of many different cell types [4]. Wound-healing studies themselves are such complex topics because of the complexity of the repair phase, which include a lot of cells and the multifaceted nature of the wound environment [5]. Understanding wound healing and examining it in detail would be important to determine how an individual will be able to improve the skin regeneration process. A wound ablation method is needed for us to examine and understand the regeneration process of a wound. Not only that, with the wound ablation method, scientists could exploit it to investigate and evaluate potential compounds for wound-healing progress. For this reason, the aim of this study is to develop a novel skin ablation method using a laser engraving machine.

In preclinical research studies, rodents, specifically mice, are the most common model organisms used to explore skin wound healing. Mice have many advantages over other models, including that they share a similar genetic makeup (99%) as humans and the availability of the established mice genetic toolbox that represents human disease models [6]. However, due to economic reasons, like high costs for daily maintenance, as well as for animal welfare issues, the scientific community continuously searches for other alternatives that are able to fit the 3Rs principle to replace, reduce, and refine experimental animal usage [7–10]. Therefore, it is important to come up with a solution to this problem. To deal with this issue, providing an alternative animal model to overcome the cost and 3R problems is always beneficial for the research community. Compared to rodents, the zebrafish model has become a good alternative animal model due to its great advantages of low expenditures and ease of handling with highly reproducible results. Although fish are lower vertebrates, they have all the classical stages of wound healing, like re-epithelialization, inflammation, cell proliferation with granulation tissue formation, and tissue remodeling, which similarly occur in humans [11]. Some studies confirm such a claim, and strongly suggest that a deep wound or injury in fish naturally undergoes a wound-healing cascade, with re-epithelialization, inflammation, granulation tissue formation, and tissue remodeling [11–14]. This wound-healing cascade occurring in zebrafish shares many similarities with classical wound healing in their mammal counterparts. The difference comes

in the initial step, which is re-epithelialization observed in fish, while it is initial blood clot formation in mammals [11]. A previous study on fish proved that superficial wounds could close within hours after wound induction, and the wound-closure speed was associated with some factors like temperature, wound dimensions, stress, and nutrition [15–18]. The rapid wound-healing ability of fish provides scientists with a good model for evaluating skin wound-healing mechanisms and an alternative method for conducting drug screening procedures to explore wound-healing potential chemicals. The standard method to explore the wound-healing properties of testing compounds has already been established in the mammalian system and is widely utilized by scientists worldwide. However, due to factors like being time-consuming, the high cost, rodent testing restrictions, and ethical concerns, the development of an alternative and simple model to address skin wound healing is considered necessary. To date, there are several studies that utilize fish as a simple model for conducting wound-healing experiments by investigating the effects of nutrition through feeding, physiology, rearing conditions, and infection routes [15,19,20]. Several different methods to conduct skin wound-healing experiments in fish have been proposed, such as a method using tissue paper to remove the mucus layer to generate partial skin wounds, or using dermal laser or biopsy punch needles to conduct full-thickness skin wounds [21] (summarized in Table A1). These methods differ on which skin tissues are damaged, and as such, different healing responses also will be triggered [21]. To induce partial-thickness wounds in fish, a previous study compared the effect of tissue paper, tissue swabs, sandpaper, and brushing on the surface of the skin of the fish. This experiment resulted in superficial skin damage caused by the tissue paper and swabbing, with the loss of the mucus layer and minor damage to the keratocytes. Meanwhile, using sandpaper and brushing of the skin caused a partial or full loss of the epidermal layer [19]. Other than such traditional methods, there are some modern tools and methods used for wound ablation.

Nowadays, there are a lot of wound-healing methods used, as mentioned before. There is a traditional method, like the scratch assay, to study cell proliferation and migration [22]. However, this method is usually only performed in cells, as it is used to examine the cell migration of cells. Meanwhile, modern wound-healing experiments utilize more advanced tools, such as the biopsy punch and dermal laser [23–27]. The challenge for skin wound-healing experiments in fish is how to control the depth and size of the wound in a consistent manner. If deeper dermal tissue is damaged, it will trigger a strong repigmentation response that leads to dermal healing, which is different from epidermal and scale regeneration [14,28]. Full-thickness models are used to study the regeneration and repair of all layers in the skin, including the scales and epidermal and dermal structures. In order to gain a full-thickness model, incisional wounds, where the skin is cut with a scalpel or razorblade, are often used to leave a narrow cut through the skin [16,17]. An incisional model is often beneficial for investigating a wound caused by a surgical incision [29]. Another method to conduct full-thickness skin injury is using a biopsy punch needle. The advantage of the biopsy punch is to induce a similar skin injury size, but the fish scale should be removed before being punctured with the punch biopsy tools [13,15]. The biopsy punch is a simple and effective diagnostic technique for wound management. However, professionals do not often use it for research because of various reasons, such as the invasive nature of the procedure or the fear of complications [23]. Another option is using a clinical dermal laser to conduct skin ablation [11,28]. Clinical dermal lasers will generate heat, which then transfers energy in the form of heat to the surrounding tissue. Wound healing then exists because of the temperature increase caused by the laser. Clinical dermal lasers also have some disadvantages, such as bleeding, pain, and infection [30]. The biopsy punch and clinical dermal laser are the most used methods for skin ablation. However, the cost of these tools is relatively expensive and not affordable for a routine lab experiment. Therefore, the development of a less expensive, easier, and more reliable method to conduct skin ablation in fish with a consistent size and depth is considered necessary. We aim to develop a novel method using a laser engraving machine in the present study as a solution for wound-healing experiments.

In addition, to facilitate the wound-size estimation, a new method was tested to perform wound-area assessment by using an artificial intelligence (AI)-based method. First, establishing and optimizing the skin ablation conditions using a laser engraving machine with a consistent size and depth of the wound, accompanied by less fish pain, was performed. Furthermore, we created the wound assessment by training the R-CNN (region convolution neural network), using either the U-Net or Mask RCNN, with thousands of skin wound images. This deep-learning method can enhance the data analysis throughput and reduce individual variation in the skin wound-area calculation. To inspect their performance, the skin wound-closure measurement performance between deep learning and ImageJ version 1.53k was examined. Although the ImageJ software has already been used as a gold standard to measure wound closure [31,32], comparison between the ImageJ and deep-learning methods can validate whether the deep-learning method is able to reach similar performance with the ImageJ method. Some conditions, like temperature, and antioxidants, like astaxanthin and vitamin C, were tested for the method validation. The present study showed a different approach than prior studies in wound healing, wherein, with the present study, a laser engraving machine was used as an alternative tool for wound ablation. Our study not only develops a novel method for laser ablation, but also proposes a new wound-area estimation method by exploiting the use of AI for the measuring tools, which differentiates our study from others. We hope that this combination approach can provide an efficient and time-saving method to conduct wound-healing studies in zebrafish. Finally, we hope that our study can turn into a new alternative for scientists to conduct wound dressing drug delivery and test potential compounds for wound healing in the future.

2. Materials and Methods

2.1. Zebrafish Maintenance

PET (pet store-purchased) zebrafish used in the wound-healing assay were obtained from a local pet store. Furthermore, for the training and optimization of a deep-learning program, three zebrafish strains (AB, PET, and TL) were used in this study and obtained from either Academia Sinica stock center (Taipei, Taiwan) or a local pet store. Zebrafish were then kept in a 10 L plastic tank and the temperature was maintained at 28 °C. The fish were fed twice a day with grown brine shrimp or with dry food for their nutrition. In maintaining healthy cultural conditions, about 50% of the water was replaced every week with fresh water. The circulating water was filtered using reverse osmosis (pH of 7.0–7.5). The dark/light cycle was maintained at 10/14 h, respectively [33]. Zebrafish were maintained in a healthy condition, manifested by being free from any signs of infection, and kept according to guidelines. All experiments involving zebrafish were performed according to the guidelines approved by the Institutional Animal Care and Use Committees (IACUCs) of Chung Yuan Christian University (Approval No. 112010, issue date 29 December 2022).

2.2. Optimization of Fish Anesthetization and Recovery

In order to perform the wound-healing assay, the administration of anesthesia was needed to immobilize the zebrafish and to reduce the pain. In this experiment, MS-222 (Tricaine Methanesulfonate) was used to anesthetize the zebrafish. MS-222 was purchased from Sigma-Aldrich (St. Louis, MO, USA). MS-222 at a 0.1% working concentration was used to immobilize the fish, and was safe enough that it did not cause any lethal effects or deaths. Furthermore, at a 0.1% concentration, it was easy for the fish to recover after being anesthetized. Initially, the zebrafish were transferred to a 0.1% of MS-222 solution until they were inactive or unable to swim. Usually, it would take around 10–30 s for the fish to be in this state. Immobilized fish were then transferred to an agarose holder to restrain the fish and prevent movement to obtain better results during the skin ablation process. Fish were positioned sideways and facing the laser upwards while they were still unconscious. Recovery was performed by transferring the wounded fish to a separate 10 L tank with clean water for 30 min until they were fully recovered and were able to swim freely in the tank.

2.3. Construction of a Laser Engraving Machine for Conducting Skin Ablation

Previous skin wound-healing experiments performed on fish, mostly using expensive dermal lasers or biopsy punches for skin wound generation, resulted in drawbacks, like high cost and operational difficulty, when using small-sized fish. To simplify this operation, establishing an alternative instrument/method to replace the dermal laser or biopsy punch was necessary. To achieve this purpose, a laser engraving machine (Zgenebio Inc., Taipei, Taiwan (<https://www.zgenebio.com.tw/english.html>) (accessed on 29 January 2024)) was tested in this study for the first time. The laser engraving machine was originally used to engrave wood or other material surfaces to the desired shape, which was equipped with a 10-watt (W) high-power CO₂ laser. This laser engraving machine consists of an XY motorized stepper that is able to precisely control the XY position of the laser beam (Figure 1A). The laser power and XY position of the laser beam can be precisely controlled by the operation software to create skin injury with a high precision and consistent size and depth. One endoscope was used to monitor and record the skin ablation process with details (Figure 1B). In addition, a digital dissecting microscope purchased from Andonstar Tech Co. (Shenzhen, Guangdong, China) was used for easy wound-size recording and visualization (Figure 1C,D). As mentioned earlier, the machine came with the Mini engraving software (Figure 1E). The software was able to control the laser beam and XY motorized stepper by adjusting some important parameters, like the laser power (indicated by watt), wound size (mm), wound shape, and the duration of laser ablation(s) (Figure 1E).

2.4. Skin Wound-Healing Assay

Adult zebrafish were randomly sampled and divided into different experimental groups (n = 10 for each group). Zebrafish with mixed gender and with age ranges from 4 to 6 months old were used. Before the laser ablation experiment, fish were acclimated in experimental tanks filled with 10 L of system water for 5 min; later, they were anesthetized by immersion in 0.1% MS-222 for 5 min. Following anesthesia, a full-thickness wound (diameter ~2 mm) was created with a laser beam with either 3- or 5-watt power for 5 s onto the left flank of the zebrafish, anterior to the anal and dorsal fin. After laser ablation, the fish were incubated with 5 ppm lidocaine to reduce the potential pain raised by the laser ablation according to the method described by Lopez-Luna et al. [34]. Fish were allowed to recover for 5 min in the system water before they were placed in their respective experimental tanks with the experimental solution, which was changed every 2 days. The wound area was monitored and measured at the predetermined time points, which were at 5, 10, 15, 20, 25, 30, 35, 40, 45, and 50 dpw (days postwound). For imaging, the fish were anesthetized, and the skin wound images were captured using a dissecting microscope from Andonstar (Shenzhen, Guangdong, China). The wound area was then measured using ImageJ software and the wound-healing effect was reported as the wound-closure percentage (WC %). ImageJ version 1.53k is a Java-based software that has been used widely for image processing [35]. First, ImageJ needed a scale to use as a standard to calculate the pixels of the images we obtained. By having the scale, we could change the standard measurement to be compatible with our image, and then the measurement could be performed by selecting the wound area and measure option [35]. The laser ablation operation procedure and protocol can be seen in the following YouTube link (<https://youtu.be/sft1udXB2wQ?si=41em-ufPDSHcFpX3> (accessed on 7 February 2024)).

2.5. Chemical Exposure

The astaxanthin and L-Ascorbic acid (vitamin C) were purchased from Sigma-Aldrich (St. Louis, MO, USA) in the water-soluble form, and then prepared as a 1000 ppm stock concentration in a liquid form and kept at 4 °C until the time of exposure. The powder form of astaxanthin and vitamin C were weighed, and both of them were easily prepared by dissolving them in distilled water to make it a 1000 ppm stock solution. After skin laser ablation, the fish were transferred to a 3 L tank filled with either astaxanthin or vitamin C at doses from 2 to 20 ppm, with n = 12 for each group. The concentration used in this

study was considered according to previous studies in another animal model, like mice. Prior studies in mice examined the effectiveness of astaxanthin for wound healing; the concentration of astaxanthin used in prior studies varied from 0.4 to 10 mg/mL. These concentrations were equal to 400–10,000 ppm [36,37]. However, because we used zebrafish, a lower concentration of astaxanthin and vitamin C was used instead (2 and 20 ppm). Meanwhile, the applied number of zebrafish was based on a previous, similar study in zebrafish [32]. The administration of antioxidant compounds was performed directly to their water tank and the treatment water was changed every 2 days to maintain the effective dose and cleanliness of the fish tank.

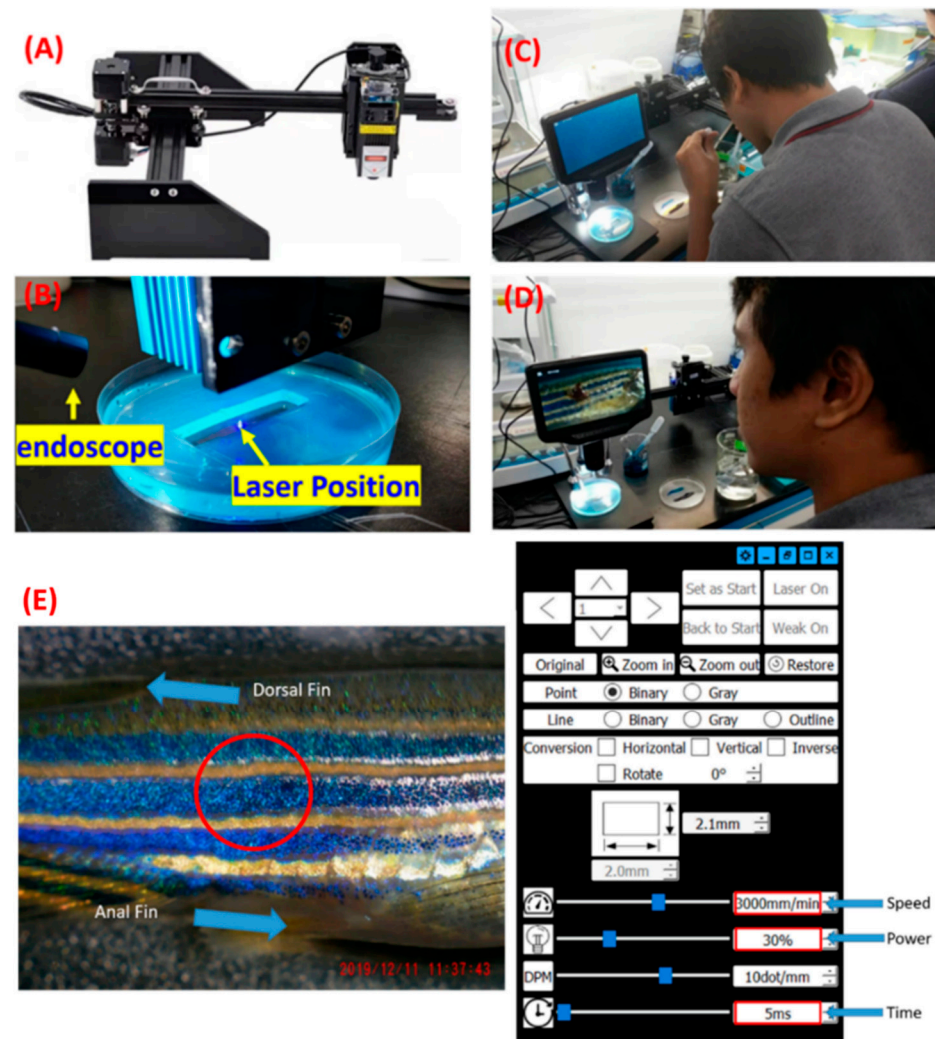


Figure 1. Overview of the skin ablation procedure mediated by the laser engraving machine. (A) The outlook of the laser engraving machine used to conduct skin ablation experiment in zebrafish. (B) The agarose holder and endoscope were used to hold the fish in position and to monitor the laser ablation process. (C) The use of methylene blue staining to mark the wounding area. (D) The wound area was recorded every five days to monitor the skin wound-healing progress. Bottom panel, creation of a precise skin wound in zebrafish by using the laser controlled by the software. (E) Left panel, the estimated location of the skin wound, indicated by a red circle, which is in the central part of the body trunk. The right panel is the control panel of the Mini engraving software, which can control the power and position of the laser beam for conducting skin laser ablation in zebrafish.

2.6. Three-Dimensional Locomotion and Fractal Dimension Test for Fish Pain Evaluation

A 3D locomotion test was performed to evaluate any behavioral alteration of the zebrafish after skin laser ablation. This assay was performed by using a polypropylene

box ($20 \times 20 \times 20$ cm) with a mirror (30×30 cm) placed at 45° from the top border of the tank to reflect all images. Later, the test tank was filled with ~ 6 L of filtered water at $25 \pm 1^\circ\text{C}$ with light-emitting diode (LED) lights on the bottom and the back of the tank as the background light sources. Afterward, a group consisting of six fish was put inside the tank and allowed to acclimatize for ~ 10 min before their behavior was recorded. The videos were captured by a Canon EOS 600D camera with a long-range zoom lens (EF-S 55–250 mm, Canon, Tokyo, Japan) that was placed ~ 6 m in front of the water tank to reduce the image distortion at the borders of the tank. Finally, the X, Y, and Z coordinates of each fish position in every frame were extracted from the videos by using idTracker version 2.1 software to calculate the movement trajectories [38]. The 3D fish locomotion tracking procedure was performed according to our previously published protocol [39], while the fractal dimension (FD) index calculation was based on several prior studies [40–42].

2.7. Computer Hardware Requirement

The proposed experimental design was implemented using the deep-learning library Pytorch on a desktop computer running the Windows 10 operating system with an Intel i9 computer processing unit (CPU), 64 Gb of random access memory (RAM), a 2 Tb SSD, and an RTX3080 Ti 12G VRAM graphic processing unit (GPU). Although a lower computer specification could also be used for the study, a high-speed GPU card is necessary to complete the design and to make the testing of the model faster.

2.8. Deep-Learning Training

The Mask RCNN and U-Net methods were used to perform image segmentation, training, validation, and testing. First, skin wound images were converted to black and white color and manually labeled as ground-truth training datasets. Later, the image argument method was applied to increase the image diversity, and then used to conduct the Mask RCNN and U-Net training to obtain two optimized Python scripts. We employed various image augmentation techniques to increase the number of training images. The experimental process for generating a wound image takes approximately 60 to 120 s, while using a computer system to generate a new wound image through image processing methods from an existing real wound image only requires 0.03 to 0.5 s. Generally, processing one real wound image into 10 training images through image processing is considered, as generating too many images from a single real image may result in minimal variation between each image, leading to a reduced impact on the training effectiveness. Taking into account the variable time cost, if considering fixed hardware costs, the fixed cost of the computer processing system is approximately USD 6000, while the fixed cost of the wound processing system is approximately USD 7000. Both in terms of time cost and equipment consumables, computer processing is more cost-effective, but real wound images are essential for the subsequent computer information processing. Training loss and test Dice curves for the skin wound-closure prediction were also measured for the performance evaluation. In total, 885, 97, and 89 images were used as training, validation, and testing datasets, respectively, to conduct the U-Net test. To increase the image diversity, images were distorted about 14-fold to generate a total of 12,390 images as a training dataset. The definition for the Dice coefficient, sensitivity (also called the recall of TPR), specificity (also called the TNR), and intersection over union (IOU) were used to evaluate the performance of the proposed method. The Dice coefficient can be defined as $DC = 2TP / (2TP + FP + FN)$, the sensitivity as $(TPR) = TP / (TP + FN)$, the specificity as $(TNR) = TN / (TN + FP)$, and the $IOU = TP / (TP + FN + FP)$, where TP, FP, FN, and TN are the true positives, false positives, false negatives, and true negatives, respectively. For the training model for the U-Net and the skin wound-size prediction model, two files can be visited, Unet_model.py and Predict.py, which are provided in Google Drive: (<https://drive.google.com/drive/folders/1byEJyRQ5OI03VMnHnJB9o3CBawbb4EwS?usp=sharing> (accessed on 7 February 2024)).

2.9. Skin Histology

Adult zebrafish were fixed in 4% paraformaldehyde/PBS for 1 day and transferred to Davidson's solution (30% ethyl alcohol, 95%, 10% acetic acid, 20% formalin, and 30% double-distilled water) for 3 days at room temperature [43]. This procedure decalcifies the hard tissues and keeps the skin in a good morphology. The decalcified samples were then dehydrated in ascending ethanol, cleared with Neo-clear (Merck), and embedded in Paraplast Plus/Paraplast HM (Leica) in a 7-3 ratio (*v/v*). The paraffin-embedded tissues were sectioned at 5 μ m intervals with a rotational microtome (HM360, Microm, NH, USA) and then stained with an H&E staining kit.

2.10. Statistical Calculation

Statistical analysis was performed by GraphPad Prism version 8.0.2 (GraphPad Inc., La Jolla, CA, USA). A *t*-test was performed to measure the significant difference in the data and Pearson's correlation test was performed to check the data correlation. Meanwhile, the behavior endpoint in the 3D locomotion test was analyzed by the Kruskal–Wallis test, followed by Dunn's multiple comparisons test. The data are presented as mean \pm SD. For the normality test in this study, the D'Agostino and Pearson correlation tests were used to find the normality of the data. Furthermore, the data were treated using nonlinear regression to obtain the 25%, 50%, and 75% wound-closure prediction. For significant differences, the data were tested by a two-way ANOVA with the Geisser–Greenhouse correction. Sidak's multiple comparison test was used to compare all treatments with the control. Furthermore, for the wound-closure percentage result, the *p* value was * *p* < 0.05, ** *p* < 0.01, *** *p* < 0.001, and **** *p* < 0.0001 for each significance level.

3. Results

3.1. Optimization of Laser Power for Skin Ablation

The best conditions for laser-based skin ablation in zebrafish need to be optimized in order to obtain consistent results. To achieve this goal, some factors, such as the laser power, wound area, survival rate, and pain reduction, should be addressed. A previous study performed by Richardson et al. (2013) showed that ± 2 –3 mm of size is optimal for the wound-healing study in zebrafish [11]. A laser will produce heat, and the heat will be transferred to the surrounding tissue in an organism, which will cause a wound. Then, this process will cause the wound-healing process to happen [30]. The laser engraving machine used in this study is capable of inducing laser beams up to 10 W (100%) of power. Laser power emitted from laser engraving machines is an important factor and is positively associated with skin wound size. The laser engraving machine was tested on wood first to obtain consistent results for the wound size. After testing it on wood, we decided to check the laser power from 1 to 5 watts as a preliminary test. Later, we found that laser power settings around 3 (30%) to 5 W (50%) can obtain a wound size around 2–3 mm in diameter consistently. Later, we examined the area in the wood produced by the laser engraving machine and compared it to the one produced in zebrafish. Using a fixed focus distance setting from the laser beam to the surface of the fish, it was revealed that the 3 W laser setting could obtain a consistent wound size when it was used on either the wood or fish skin surface, with a very low inter-assay variation (around 5% coefficient of variation, Figure 2A). As seen in Figure 2A, the area of the wound produced by the laser engraving machine was consistent in both the wood and fish, which was around 2–3 mm².

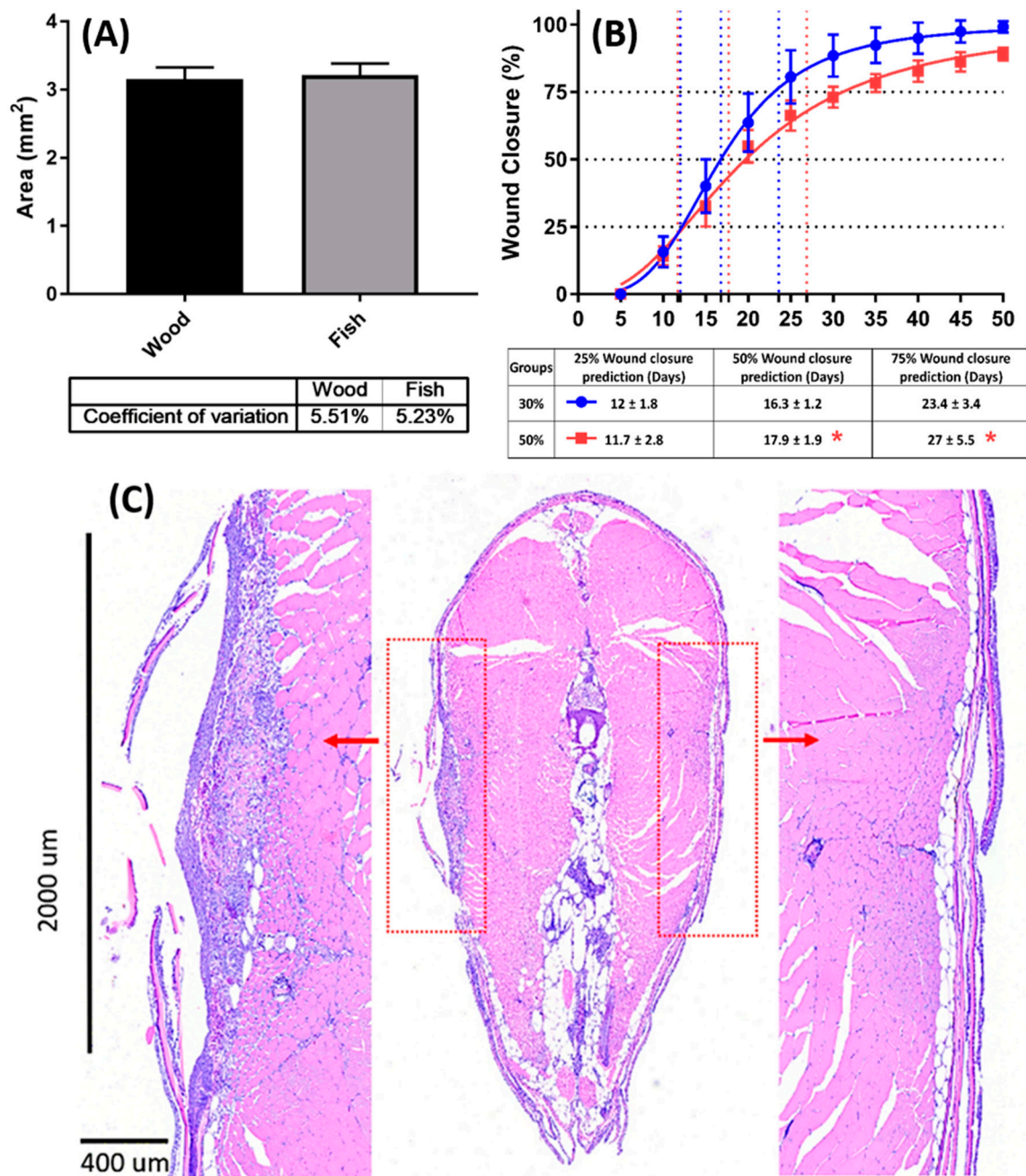


Figure 2. Wound-area and wound-closure percentage on zebrafish using the laser engraving machine. (A) Test for the consistency of the wound area created by the laser. Before the experiment, the wound size was first tested on wood, and later tested on the fish skin. The data are expressed as mean \pm SD and were analyzed by an unpaired *t*-test. (B) Time chronology of the skin wound-area recoveries of the zebrafish. The data are presented as mean \pm SD, $n = 10$ for each group (* $p < 0.05$). The data were tested using nonlinear regression to obtain the 25%, 50%, and 75% wound-closure prediction. (C) Skin wound histology in the paraffin section with H&E staining. The left side shows a skin wound and the right side shows the unwounded control. The full-thickness skin wound after receiving a 3W laser was estimated as 2000 μ m in width and 400 μ m in depth.

Next, the survival rate of the fish was tested after receiving laser ablation with different power settings. The results showed no signs of fish lethality after receiving either the 3 or 5 W laser settings. However, the stronger laser power given by the 5 W setting can produce increased skin damage and take more time for the skin wound to close (Figure 2B).

The fish that received the 3 W optimized laser power, on the contrary, displayed a smooth sigmoid wound-healing curve that was able to complete skin wound healing within 50 days. The skin wound-healing curve for the 3 W wounded zebrafish showed a faster wound-healing process (blue color), while the 5 W wounded zebrafish showed a relatively slower wound-healing process (red color) (Figure 2B). Moreover, the wound-healing performance was investigated using the curve-fitting method to predict the time to reach 25%, 50%, and 75% wound closure. There were significant differences between the 3 W and 5 W laser on the wound-closure percentage. For example, the 3-watt group only needed around 16 days to close 50% of the wound; meanwhile, the 5-watt group needed longer to close the wound (18 days). This indicates that the 5 W laser imparted a more severe wound and needed more days to be fully healed compared to the less severe wound caused by the 3 W laser power. Fish groups receiving the 3 W laser showed faster skin wound closure; within 16 days, half of the wound was already closed. Based on all collected data, this study revealed that a 3 W laser is the safest and most optimum power used to induce skin wounds in zebrafish. The faster wound-closure percentage and consistent wound produced by 3 watts make it the best condition for skin ablation in zebrafish. In addition, histological sections were performed to examine the size and depth of the skin wound. By paraffin sections and H&E staining, the skin thickness was estimated at around 150–200 μm on the unwounded side (Figure 2C, right panel), while it could reach 400 μm in depth and 2 mm in width after receiving the 3 W laser ablation (Figure 2C, left panel). Those results confirmed that the optimized 3W laser power setting can induce a full-thickness skin wound in zebrafish with a consistent initial wound size, smooth skin closure process, and less lethality.

3.2. Evaluation of Fish Pain after Laser Ablation

As one of our main concerns in developing this laser-based skin ablation method, pain assessment is required to evaluate the pain experienced by the test fish during and after laser ablation, and to ensure the compatibility of this procedure with an ethical point of view. Unlike in humans, the assessment of pain in animals cannot be obtained by direct communication; therefore, an indirect method like behavior assessment was used to evaluate the potential pain response in zebrafish. Since pain is an adverse physiological experience resulting in learning, memory formation, and altered strategic decision-making, in animals, it is often indicated by behavioral alterations and the performance of abnormal or unusual behaviors [44,45]. Here, at ~1 h after skin ablation, behavior alteration was assessed by using a 3D locomotion test. Groups of fish that were given a wound by 5-watt laser power showed rather abnormal behavior. This behavior abnormality was indicated by statistically low levels of the fractal dimension (FD), average speed, and total distance traveled at the top (Figure 3A,B,D), as well as a high level of meandering (Figure 3C). The FD, a mathematical index for locomotion complexity evaluation, has been used for behavioral monitoring, including pain evaluation [42,45]. Generally, a healthy fish displays a higher FD value than a sick or pain-suffering fish. In this study, the 5-watt group showed a significantly lower level of FD value ($*** p < 0.001$) compared to the 3-watt and control groups (Figure 3A). In line with the previous study, a substantial reduction in the activity and swimming distance, resulting in a reduction in the complexity of movement as well as space use, was displayed by adult zebrafish during pain [42]. The increment in meandering also indicated that the treated fishes were in a high anxiety state that might have been caused by the wound [46]. As can be seen in Figure 3C, the 5-watt group showed a significantly higher level of meandering ($** p < 0.01$) compared to the 3-watt and control groups. On the contrary, the fish treated with a 3W laser displayed similar behavior endpoints with the control. According to the result, there are no significant differences in the 3-watt group, which means that the behavior of 3-watt-treated fish and control are similar. Taken together, laser setting at high power (5 W) caused more pain to the fish, while the low power (3 W) did not lead to the behavior alteration, indicating the absence of pain or less pain in the treated fish after ablation with the laser at that power level. Therefore,

based on these results, this study concluded a 3W laser power was identified as the optimal condition for the skin ablation experiment due to inducing less pain in adult zebrafish.

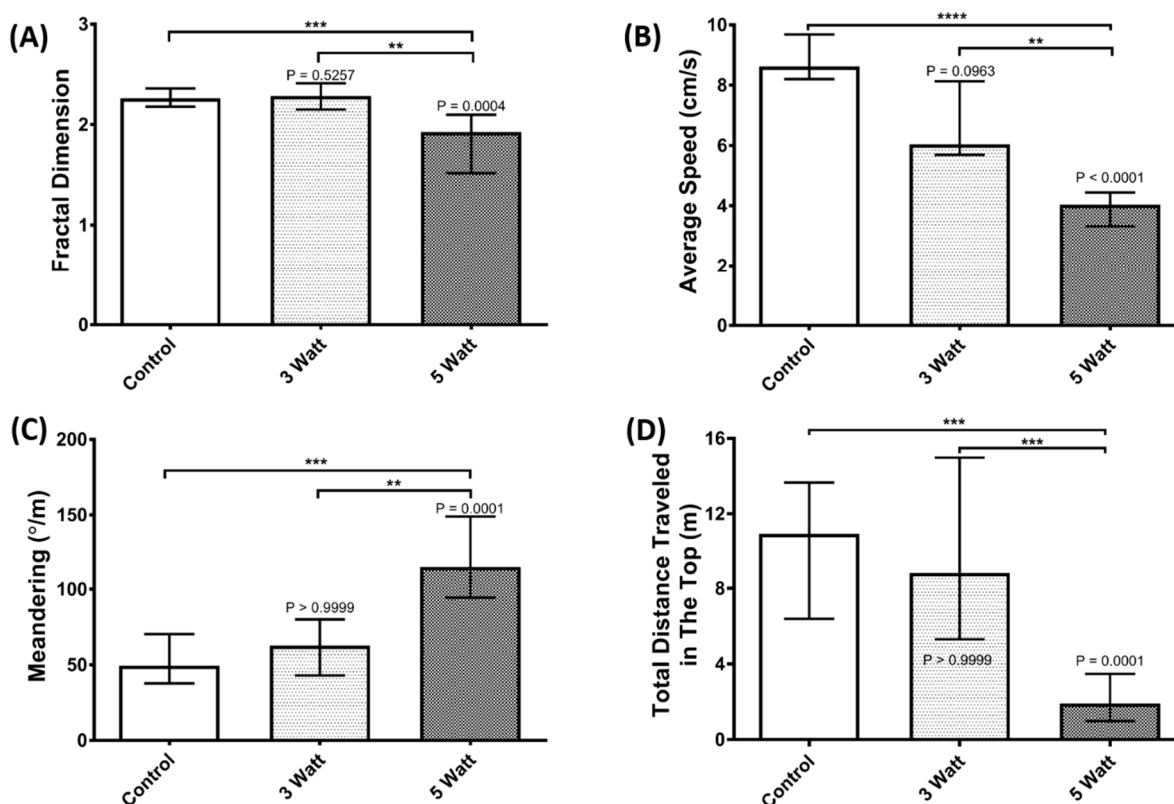


Figure 3. Behavior endpoints were obtained from the 3D locomotion assay of zebrafish after 1 h of skin ablation with either 0 (control), 3, or 5 watts of power. (A) Fractal dimension, (B) average speed, (C) meandering, and (D) total distance traveled at the top were calculated. The data are expressed as the median with the interquartile range, and were analyzed by the Kruskal–Wallis test, followed by Dunn’s multiple comparisons test. Two replicates with a total sample size of 12 fishes were applied in this experiment (** $p < 0.01$; *** $p < 0.001$; **** $p < 0.0001$).

3.3. Skin Wound-Closure Measurement by Deep Learning

The previous method to perform skin wound-closure quantification was solely based on the ImageJ method. Since the manual interpretation of the wound-healing area is easily affected by the opinions of the interpreter, it is better to establish an automated wound-area interpretation system to minimize the potential biases from human operational errors. In clinical practice, image segmentation and deep-learning methods have been successfully applied to perform skin cancer or skin wound-size estimation [47,48]. However, such an approach has not been reported in zebrafish. Because the contour of the wound area is very irregular and the boundary is blurred, traditional image edge detection, segmentation, and others relying on hand-crafted algorithms will not easily obtain accurate results. Moreover, if the hand-carved algorithm is applied to zebrafish species with different pigmentation patterns in the skin, the detection accuracy will be reduced, and a new algorithm must be redesigned manually to adapt to the new fish species. Therefore, in this study, a supervised machine-learning method was adopted to automatically learn the interpretation rules to establish an easily learnable and adaptable wound-contour interpretation system. After judging the contour of the wound, the relationship between the image area and the actual wound area was calculated by traditional image processing methods, and the absolute wound area served as the ground truth was calculated based on the images. The workflow of establishing a machine-learning system is summarized in the following cartoon picture (see Figure 4 for the system architecture).

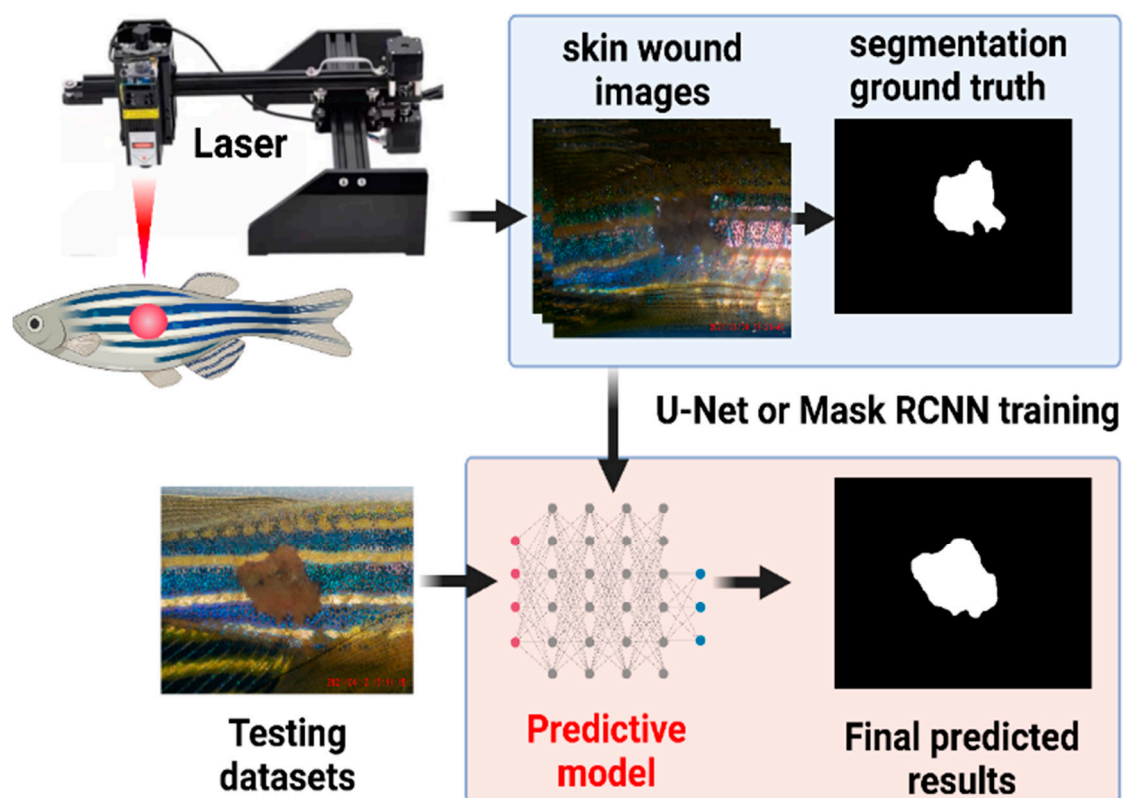


Figure 4. Experimental workflow for skin wound-healing area measurement by using a deep-learning approach. The wound atlas collected in the previous stage will be divided into three parts: the training set, validation set, and testing set. The pictures of these three sets are mutually exclusive. The training set is used to train the neural network model, and the validation set is used to verify the training results during the training phase. The test set is used to evaluate the performance of the system after the training.

3.3.1. Image Collection and Preprocessing

After skin ablation, pictures were taken of the fish with a suitable visible light source and shooting distance. The photographed images are marked with the wound area using the image-processing tool of ImageJ. ImageJ is a Java-based open-source software for image processing into an invaluable laboratory tool. ImageJ can be used to display, edit, and process an image. They incorporate useful tools for image processing, like histogram manipulations and standard image filters. Not only that, but they also have a lot of macros and plugins which are helpful for image processing [35]. The marked picture serves as the ground truth for the training and verification. We initially collected around 1071 images, covering different skin wound sizes, which were taken at a fixed magnification and pixel dimension. Later, the wound areas and backgrounds were manually marked and converted into white and black colors, respectively. The dataset was first divided into 885 training images, 97 validation images, and 89 testing images. When the image set was not big enough, image augmentation was used to increase the size of training images [49,50]. The image augmentation procedures were performed on the training images to augment the images from 885 to 12,390. The image augmentation methods performed here include cropping, flipping, grid distortion, elastic transform, optical distortion, as well as brightness contrasting [51]. The same augmentation procedures were also performed on the validation images to augment the images from 97 to 1455.

3.3.2. Model Training

There are several reported methods currently available that may be suitable for marking the contour of the skin wound in zebrafish. In this experiment, we evaluated two

deep-learning methods, the U-Net [52,53] and Mask R-CNN [54]. The U-Net is a generic deep-learning solution for image detection and segmentation, and can be used for biomedical image data analysis [52,53]. The U-Net uses the U-shaped network structure to first capture the features of the images and reconstruct the required partitions based on these features. The difference from general segmentation is that the fish wound map contains fish scale lines and irregular fuzzy wound boundaries, so it is difficult to use the semantic features of the image to identify the contour of the object. Therefore, U-Net's method of fusing low-level and high-level image features may have a chance to successfully mark the contours of fish wounds.

The U-Net architecture contains a U-shaped path. The image enters one end of the U-shaped network to go through the encoding part of the network (also called the down path). The encoding part is used to capture the features of the input images. Then, the information of the input image is sent to the decoding part (also called the up path) to construct the segmentation image. In addition to this, the direct connections are used to pass the precise localization information of the features in the encoding part to help the decoding part in generating the segmentation. The major components of the encoding part of the U-Net are the convolution layers and max-pooling layers. The convolution layers contained in the encoding part use a set of filters (also called kernels) to extract the features. The output features of a convolution layer are usually passed to another convolution layer for extracting higher-level features. After several convolution layers, the max-pooling layers are used to reduce the size of the features so that useless features can be eliminated. A typical max-pooling layer selects the maximum pixel value from each group of four pixels, and the selected pixels are arranged to form the pooled feature map. On the other side, the decoding part needs to convert a compressed feature map to a high-resolution segmentation image. The U-Net uses the transposed convolution layers to perform the upsampling work. The transposed convolution (also called deconvolution) is the opposite process of convolution. Because a convolution operation can be expressed as a matrix multiplication of a filter matrix and an input image (denoted as a matrix), the reversed convolution operation can be performed by the matrix multiplication of the transpose filter matrix and an input feature map. This is why the reversed convolutional operation is called a transposed convolution. Methods such as the R-CNN first use image semantic features to detect the area of the object and then send this area to another network to mark the area. Whether this type of method can effectively find out the wound area that does not have a specific shape for object detection is a key issue. Those color-converted images were saved as the ground truth for the segmentation training. Later, both the original images and the marked and color-converted image ground-truth image pairs were conducted for 1000 epochs of the R-CNN training with a U-Net network containing four down and four up hidden layers. After completing the image and model training, the testing image datasets were uploaded for the wound-size prediction.

3.3.3. Test Results

This study was able to write an image area calculation program, and later use this program to calculate the area of the wound with the wound map marked with the boundary area. Comparing the manually calculated area and the program-calculated area, the overall performance of our system was established. Finally, the data obtained from deep-learning prediction and the data collected from the ImageJ manual measurement were compared and subjected to correlation validation. Later, deep learning's performance was evaluated by comparing the Dice and loss curves in the training and validation processes. For training, the Dice coefficient increased exponentially after 100 steps, and already reached the maximal plateau after 2000 steps. The loss curve also already reached the minimal level after 2000 steps. For validation, the Dice coefficient reached the maximal plateau after 2000 steps. The loss curve also showed a minimal level after 2000 steps. Interestingly, the Dice and loss curves for either the gray or RGB color images displayed no significant difference for the training process (Figure 5A,B). The Dice and loss curves for the RGB

color images also displayed similar performance with the gray images for the validation process. This result suggests the U-Net deep learning used in this study might recognize skin pigmentation patterns rather than skin color. Similar results also can be found for the Mask RCNN training and validation (Figure 5C,D).

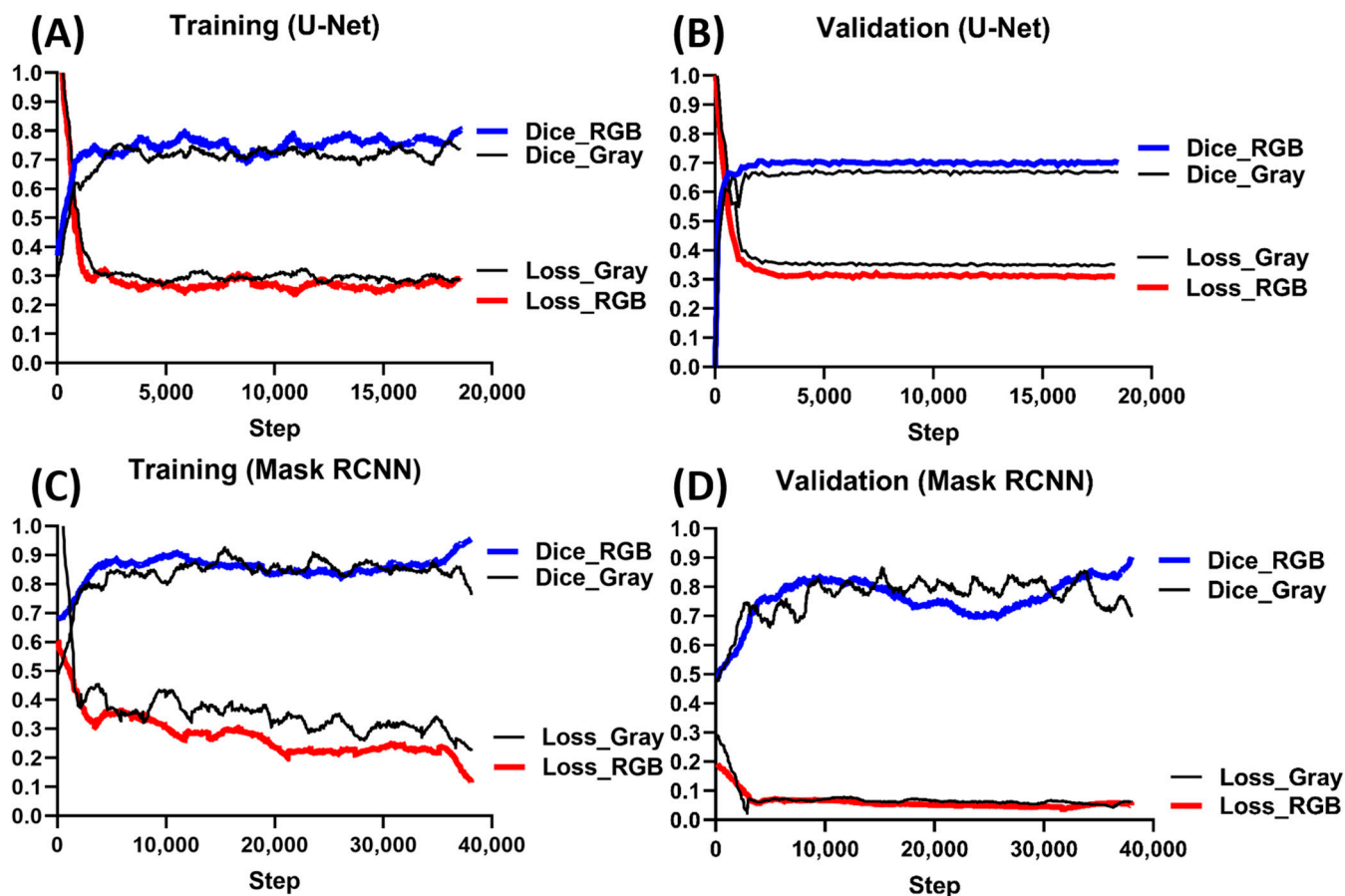


Figure 5. Training loss and test Dice curves for skin wound-closure prediction by using either U-Net or RCNN. In total, 885, 97, and 89 images were used as training, validation, and testing datasets, respectively, to conduct deep learning-based wound-size prediction. To increase image diversity, images were distorted about 14-fold to generate a total of 12,390 images as a training dataset. (A) The Dice and loss curves for the U-Net training process by using gray or RGB skin images. (B) The Dice and loss curves for the U-Net validation process by using gray or RGB skin images. (C) The Dice and loss curves for the Mask RCNN training process by using gray or RGB skin images. (D) The Dice and loss curves for the Mask RCNN validation process by using gray or RGB skin images.

In addition, in this study, we found that a good laser ablation position in the central body part is crucial for precise wound-area prediction by deep learning. If the laser ablation was not given in the central part of the fish body, then the overall U-Net prediction power would decline dramatically due to the misidentification of the skin wounds with background noise. To avoid any ambiguous data, only images with central skin wounds were selected to conduct the skin wound-size prediction.

For the testing process, we compared the size of the predicted wound area with the ground truth, and later four endpoints were used for the performance evaluation in terms of the Dice coefficient, IOU, sensitivity, and specificity based on a previous semantic segmentation study [55]. For the PET zebrafish strain, the image color contributed less to the wound, since there was no significant difference for all four major endpoints between gray and RGB images (Table 1). This result supports the previous hypothesis proposed based on data collected from the Dice and loss curves in Figure 5. These interesting findings

led us to investigate further whether the U-Net deep-learning network built in this study could be used for other zebrafish strains with different body colors or strip patterns. For the body-color test, the golden strain (carrying *slc24a5* gene deficiency) was selected, since its body showed a more intense yellow color than the AB strain, but with a similar pattern. The result showed the optimized neural networking built up with the PET strain by the U-Net was still able to be applied to the golden strain with a relatively good prediction power (Table 1).

Table 1. Comparison of prediction power of the U-Net and Mask RCNN for skin wound healing in zebrafish. For statistical differences in sensitivity and specificity, the data were tested using a one-way ANOVA test, followed by Tukey’s post hoc test (a) used as a label; different letters beside the results indicate a statistical difference with $p < 0.05$. The data in this table are all expressed as mean with SD.

Strain	Image Color	Dice Coefficient	IOU	Sensitivity	Specificity	n
U-Net method						
Zebrafish PET strain	RGB	0.815 ± 0.242	0.737 ± 0.251	0.801 ± 0.265 (a, d)	0.996 ± 0.004 (a)	75
	Gray scale	0.781 ± 0.276	0.703 ± 0.281	0.762 ± 0.300 (a, c)	0.997 ± 0.004 (a)	75
Zebrafish Golden strain	RGB	0.411 ± 0.356	0.328 ± 0.318	0.400 ± 0.381 (b)	0.992 ± 0.012 (b)	79
	Gray scale	0.648 ± 0.313	0.548 ± 0.308	0.592 ± 0.330 (c)	0.997 ± 0.005 (a)	79
Zebrafish TL strain	RGB	0.907 ± 0.116	0.846 ± 0.157	0.951 ± 0.116 (d)	0.995 ± 0.002 (a, b)	60
	Gray scale	0.882 ± 0.162	0.815 ± 0.187	0.878 ± 0.185 (a, d)	0.996 ± 0.003 (a)	60
Mask RCNN method						
Zebrafish PET strain	RGB	0.774 ± 0.332	0.716 ± 0.318	0.792 ± 0.340 (a, d)	0.996 ± 0.004 (a)	75
	Gray scale	0.759 ± 0.334	0.696 ± 0.324	0.757 ± 0.343 (a, c)	0.997 ± 0.002 (a)	75
Zebrafish Golden strain	RGB	0.431 ± 0.444	0.390 ± 0.413	0.421 ± 0.444 (b)	0.997 ± 0.005 (a)	79
	Gray scale	0.352 ± 0.439	0.320 ± 0.408	0.353 ± 0.449 (b)	0.997 ± 0.006 (a)	79
Zebrafish TL strain	RGB	0.872 ± 0.226	0.819 ± 0.234	0.916 ± 0.221 (a, d)	0.996 ± 0.003 (a)	60
	Gray scale	0.884 ± 0.188	0.825 ± 0.201	0.937 ± 0.183 (a, d)	0.995 ± 0.003 (a, b)	60

For the PET strain, based on the U-Net, a very good performance on skin wound-size prediction was observed when compared to the ground truth. Based on 89 images collected from zebrafish by 5 to 50 DPW, it was revealed that there was no significant difference between the ground truth and prediction, which was validated by using a paired *t*-test ($p = 0.6972$, Figure 6A,C). Later, we investigated whether the U-Net network prediction power displayed any consistency for different sizes of wounds. By using the XY correlation plot, it was revealed that the prediction error rate displayed a relatively low level for bigger skin wounds and a high level for smaller skin wounds (Figure 6B). For middle-to-big wound ($>2 \text{ mm}^2$) area prediction, the error rates were less than 25%, while they could reach around +125% to −100% for small wounds of less than 2 mm^2 . Figure 6C shows some examples of the ground truth and predicted area comparisons at different time points after the skin ablation. Taken together, the optimized U-Net performed very well for the skin wound-area and morphology prediction. Only significant over- or underestimation was found in very small skin wounds. Those errors can be ignored, since they contributed less to the skin wound-closure percentage, which is divided by the relatively big wound skin at 5 DPW.

After testing the PET strain, it was interesting to know whether the trained U-Net was still able to measure skin wounds from other strains, like the golden or TL zebrafish strains. Golden zebrafish that carry the *slc24a5* gene deficiency have a phenotype of golden-like skin/scales. Their color is different from the PET zebrafish, and was used as an outlier to test the power of the U-Net. The results confirmed that the U-Net could still predict the skin wounds on the golden zebrafish. Table 1 shows that the specificity and sensitivity

of the U-Net in predicting skin wounds for golden strain are quite high, which is around 0.9 and 0.7. This proved that, even with different skin colors, the U-Net was still able to predict skin wounds in zebrafish. Next, we tested whether the U-Net still could precisely measure the skin wounds for zebrafish strains with different pigmentation patterns. To validate this hypothesis, TL zebrafish with a leopard-like pattern on their scales were tested. The results demonstrate that the U-Net was still able to give a good result in measuring the skin wound size in the TL zebrafish, with around a 0.9 sensitivity; the 0.9 specificities were quite similar to the PET zebrafish. From this result, it is concluded that the trained U-Net model proves to be a good deep-learning machine for measuring wounds on a broad range of zebrafish strains.

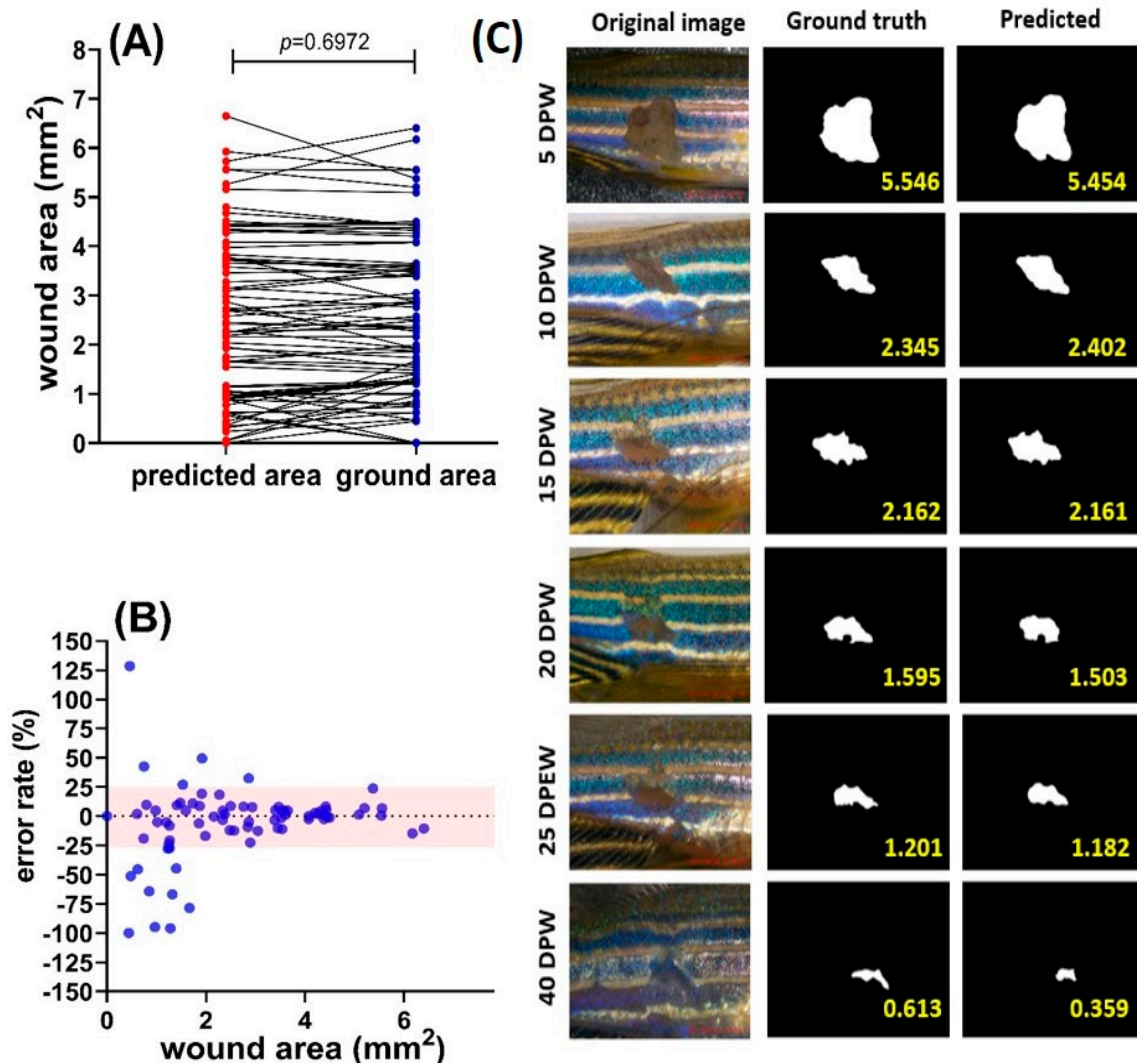


Figure 6. Test the power of deep learning in detecting the potential wounds in fish by using the optimal U-Net. **(A)** Comparison of the skin wound-area size between deep-learning prediction (red color) and ground truth (blue color). **(B)** The correlation between the wound-area size and wound-area prediction error rate. **(C)** Time chronology images showing the high similarity between the ground truth and predicted skin wound size in zebrafish using U-Net. DPW, days postwound.

3.4. Skin Wound-Closure Measurement Validation

After the establishment of the laser ablation and deep-learning methods for the skin wound-area measurement, it is important to conduct a data validation step to compare the deep-learning prediction power with the ImageJ-based manual measurement method. The skin wound-closure curve generated by the U-Net-based deep learning- and ImageJ-

based methods were compared side-by-side. In the ImageJ software, before measuring the wound, size calibration was conducted with a scale bar to find the pixel to distance relationship. The image of the zebrafish wound area was then analyzed using the ROI manager by selecting the skin wound area as the target. Selected wound areas could be measured with a measure option that is in the ROI manager menu. We hypothesized that the optimized deep-learning model was able to predict the skin wound size with a high precision and automated manner. To validate this hypothesis, some conditions, like ambient water temperature and antioxidants able to enhance or delay wound healing in rodents, were used.

3.4.1. Temperature Conditions and Their Effect on Wound-Healing Process

Various environmental factors can affect the quality of animal life; one of them is temperature. Temperature is also important in the wound-healing process, and higher or lower temperatures can affect the speed of wound healing in animals. Temperature can affect fibroblastic activity and keratinocyte migration and, therefore, plays an important role in skin wound healing [56,57]. To prove this concept in a zebrafish model, we examined how high (35 °C), ambient (25 °C), and low (15 °C) temperatures affect the wound-healing process in zebrafish. Zebrafish skin was ablated by a 3W laser beam; then, they were transferred to a temperature-controlled oven with the temperature set at either 35 °C, 25 °C, or 15 °C.

Other than the 50% wound prediction, in this study, we also proposed another two important endpoints of either 25% or 75% wound closure that could be used to fully cover the early (25%), middle (50%), and late (75%) wound-closure events for re-epithelialization and inflammation, granulation tissue, and the maturation process. By using the curve-fitting method, we found it was very useful for performing skin wound-closure evaluation by using this multiple-endpoints method. Basically, skin wound-closure kinetics obtained by the U-Net prediction and manual measurement using ImageJ were consistent, showing faster wound closure in the higher-temperature group and much slower in the low-temperature group (Figure 7). Low temperature has been reported to delay tissue necrosis, macrophage response, the clearance of bacteria, and finally slow down skin wound closure [58]. The time for skin to reach 50% of the wound closure was also investigated. The high-temperature (35 °C) condition could speed up the wound healing, taking ~12.2 days to reach 50% wound closure, while it took ~16.78 days for the control and ~54.4 days for the low-temperature group (the p value for each significance level was * $p < 0.05$; ** $p < 0.01$; *** $p < 0.001$; **** $p < 0.0001$). This means that the 15 °C condition delayed the wound-healing process significantly, as 50 days were needed for the zebrafish to reach a 50% wound-closure condition. Furthermore, by evaluating the 25% wound-closure endpoint, we could check their early wound-healing process. It took ~6.3 days for the high-temperature group (35 °C), ~11.9 days for the control, and ~16.8 for the low-temperature group (25 °C). We can see that, even in the early wound-healing process, temperature already played an important role. High temperatures were significantly faster compared to the other group, while low temperatures already took a lot of time to close the wound (Figure 7). These results clearly demonstrate that skin wound healing in zebrafish is temperature-dependent, and the ambient water temperature should be well controlled and reported when conducting such experiment for better data consistency. In addition, it also can significantly save time to conduct faster wound healing-potential evaluation by assessing the early 25% wound-closure endpoint. By performing the 25%, 50%, and 75% wound-closure testing, this protocol could help us to choose which process of early, middle, or late wound healing we want to focus on. Furthermore, the performance of the AI developed for wound measurement is working great, as the results are still comparable to each other.

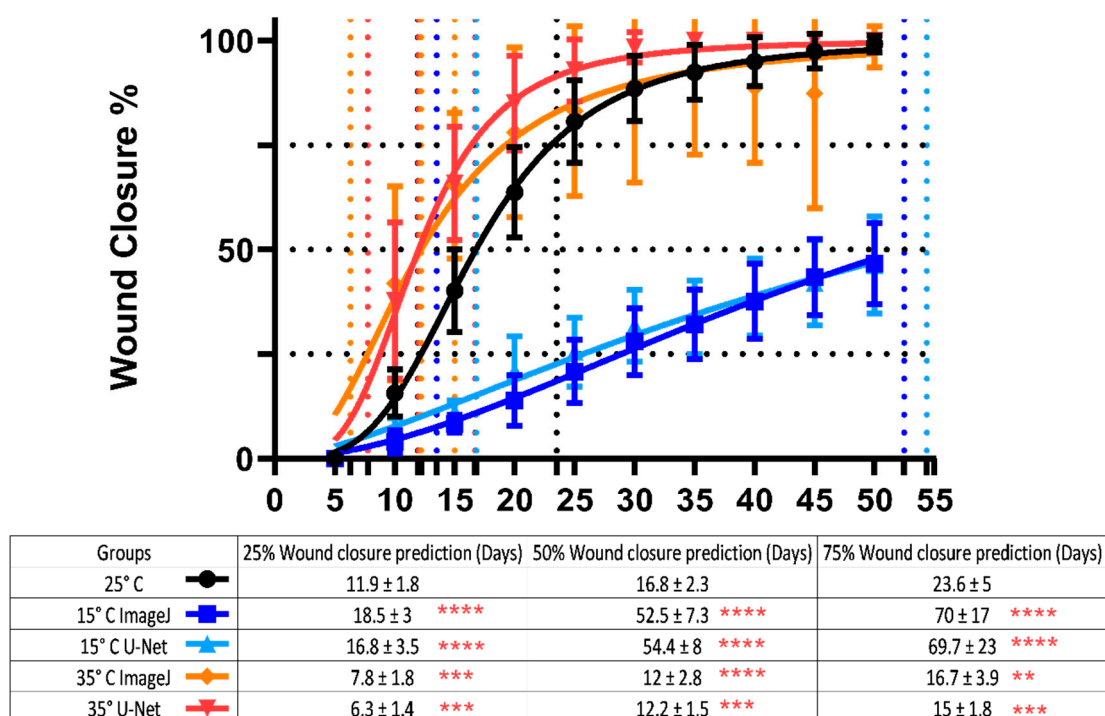


Figure 7. Wound-area and wound-closure percentage on zebrafish using the laser engraving machine. The wound-healing closure percentage curve that was affected by low (15 °C) and high (35 °C) temperatures. There are two sets of data measured manually with ImageJ and with deep-learning U-Net prediction. The data are presented as mean ± SD, n = 12 for each group. For statistical differences, the data were tested by a two-way ANOVA with the Geisser–Greenhouse correction. Sidak’s multiple comparison tests were used to compare all treatments with the control, with n = 12 for each group (* $p < 0.05$; ** $p < 0.01$; *** $p < 0.001$; **** $p < 0.0001$).

3.4.2. Antioxidants Test to Speed up Wound-Closure Process

Towards achieving a consistent method in wound healing, antioxidants such as astaxanthin and vitamin C (ascorbic acid) as a positive control were used. This was also performed to validate the deep-learning performance of the skin wound-size prediction. Both astaxanthin and ascorbic acid are strong antioxidants that are already known for their properties in boosting the skin wound-healing process [59–62]. Here, the astaxanthin and vitamin C were added directly to the water where the fishes were to check whether the compounds could enhance the wound-healing process or not. As expected, both astaxanthin and vitamin C could enhance the skin wound-healing process in zebrafish, as seen in the curve. The curve produced by both astaxanthin and vitamin C showed an enhanced wound-closure process. This means that both astaxanthin and vitamin C are responsible for the wound-healing process. In the astaxanthin-treated fish, it only took ~11 days for 20 ppm and ~13 days for 2 ppm to reach 50% wound closure, while the untreated zebrafish took 16.8 days to close 50% of the wound (Figure 8A). Astaxanthin-treated fish showed a significantly faster wound healing compared to the control fish. A higher concentration of astaxanthin (20 ppm) could reach a more pronounced wound closure-promoting effect, which was judged by either 25% or 50% wound-closure endpoints (Figure 8A). Furthermore, another tested antioxidant, vitamin C, showed similar results with astaxanthin, where it sped up the overall wound-healing process in zebrafish. It only took ~12 days for 20 ppm and ~14 days for 2 ppm to reach 50% wound closure compared to the control, which took ~16 days (the p value for each significance level was * $p < 0.05$; ** $p < 0.01$; *** $p < 0.001$; **** $p < 0.0001$) (Figure 8B). The results also confirmed that astaxanthin performed better than vitamin C in boosting the skin wound closure in zebrafish. Taken together, all evidence collected in this study proves that this laser-based skin ablation method indeed

offers an alternative and simple method for skin wound-healing studies on zebrafish. The combinational use of deep learning-based wound-size measurement method also gives consistent results which are comparable to those obtained from the manual calculation. The result proves that the trained U-Net deep-learning model can work properly to measure the skin wound area in zebrafish automatically for the first time.

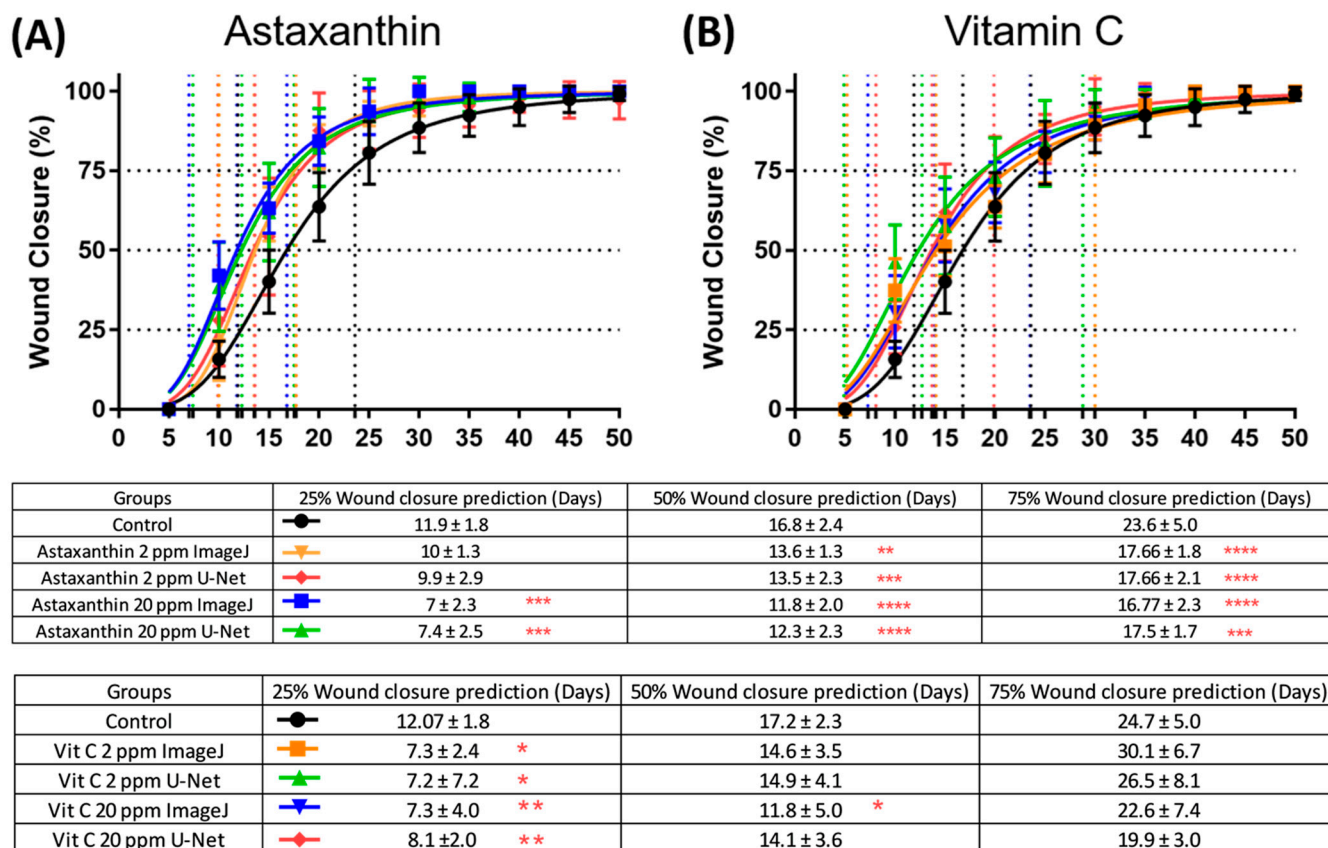


Figure 8. Validation of antioxidants as a strong positive control to promote skin wound healing in zebrafish after performing laser ablation. (A) Wound-healing closure percentage curve of zebrafish treated with both high and low doses of astaxanthin. (B) Wound-healing closure percentage curve of zebrafish treated with both high and low doses of vitamin C (ascorbic acid). The data are presented as mean ± SD. The data were tested using nonlinear regression to obtain the 25%, 50%, and 75% wound-closure predictions. For statistical differences, the data were tested by a two-way ANOVA with the Geisser–Greenhouse correction. Sidak’s multiple comparison tests were used to compare all treatments with the control, with $n = 12$ for each group and each concentration (* $p < 0.05$; ** $p < 0.01$; *** $p < 0.001$; **** $p < 0.0001$).

4. Discussion

4.1. A Laser Engraving Machine-Based Method Has Been Established to Create Consistent Skin Wounds in Zebrafish

All disruptions at the cellular level, anatomical level, and functional level of a living tissue could be defined as a wound. There are different types of wound injuries, such as chemical, physical, thermal, and microbial injuries [63,64]. When the skin is torn, cut, or burned, or when a blunt force causes a contusion, it will cause the structural integrity of the skin to be compromised. This is when wound healing would happen in order to keep the hemostasis in an organism and prevent further injuries to it [63,64]. Wound healing is a biologic process that is naturally occurring in an organism, where it regenerates injured parts to regain its normal condition [3]. This process is so significant that scientists started to discover more of the details of the wound-healing process, looking for efficient means to hasten and speed up the sound healing process. There are several established methods

in the wound-healing assay, such as methods utilizing cell lines as a standard in vitro technique for proving collective cell migration by removing the cells through mechanical, thermal, or chemical damage [65]. In vitro techniques like this were used to examine the cell migration in cell-free areas, which is one of the significant indicators of the wound-healing process [66–69]. However, the full-thickness skin wound healing containing the epidermis–dermis interaction might be unable to be recapitulated by a simple in vitro assay. In this consideration, rodents, like mice or rats, or even big mammalian animals, like pigs, were reported as good models to examine the skin wound-healing process and mechanism [6,70,71]. Moreover, there are some techniques that make use of more advanced tools, such as clinical dermatology lasers and biopsy punches, to investigate wound healing [11,14,23,26]. However, the clinical dermatology laser is relatively expensive and might be unaffordable to many laboratories. Furthermore, there is also a significant limitation on the reproducibility of the data because of the high cost, limited number of test animals, and ethical concerns about the use of rodents. Thus, in this consideration, it is important and necessary to establish a simple and cost-effective method to create consistent skin wounds in the target animal, as well as to establish a high-throughput method able to qualitatively measure skin wounds in an automatic manner.

The most important innovation for this study is that we provided an optimized laser engraving machine-based method as an alternative approach to the clinical derma laser or biopsy punch to create skin wounds. By utilizing a low-cost laser engraving machine, we were able to produce very consistent skin wounds in zebrafish with less pain and adverse effects (mortality) for the treated fish. The uniform power output also made it possible to generate a uniform size of skin wounds and greatly reduce the potential individual variation for wound sizes. Moreover, using this optimized protocol, full-thickness skin wounds could be consistently, quickly, and reproducibly introduced on the flank of adult zebrafish. The skin wounds generated by this laser-based method could be fully healed within 30 to 40 days, which is quite fast. This might be because the wound produced in this experiment comes from a laser, which produces heat and physical cuts from the laser [30]. Some studies showed that using a laser could result in faster wound healing, since the light and heat could induce collagen bonds strong enough to support moderate tension [30,72]. Previously, the laser has been used for tissue volatilization (the ablative technique) and thermal diffusion in skin resurfacing and tissue welding. Using this method, the wound-healing process becomes faster and more evident [73].

In this study, the optimal laser power of 3 watts was validated to generate skin wounds with a consistent size and depth, as well as to induce less animal suffering. This result was similar to other studies that used a laser power range of 1–10 watts [74,75]. Utilizing the 3-watt laser power, the full-thickness wound was consistently generated onto zebrafish. As mentioned earlier, heat from a laser could enhance the wound-healing progress in this experiment. This is also supported by a previous experiment that used a ruby laser on the dorsum of mice. This phenomenon could happen because of the laser biostimulatory effect, creating mechanical and burn injuries. The laser-treated side showed accelerated healing and greater epithelial proliferation [76,77]. Furthermore, another previous study on wound healing also proved that the He-Ne laser was found to increase the rate of wound closure in rats and mice [78–80]. These studies supported the current findings in this study that using 3 watts of laser power could consistently generate the wound as well as promote the wound to be fully healed within around 30–35 days. Interestingly, a recent study also proved that the laser is an effective therapeutic modality to promote the healing of some wounds. The effects of this therapeutic technique are related to the decrease in inflammatory cells, increased fibroblast proliferation, angiogenesis stimulation, the formation of granulation tissue, and increased collagen [81]. Moreover, another study also proved that laser therapies might improve the wound-healing process and reduce swelling and pain after tooth extraction [82].

4.2. Three Important Endpoints Were Proposed to Exam the Early, Middle, and Late Skin Wound-Healing Event in Zebrafish

Previous *in vivo* wound-dressing studies were also conducted in mammals, such as pigs, rodents, or rabbits, which are limited by the drawbacks of a low throughput, high cost, and debate on the violation of animal rights [83–85]. Following the 3Rs guideline [9], the aim was to establish zebrafish as a simple and alternative model to conduct skin wound-healing studies. Compared to higher forms of vertebrate models, zebrafish provide a relatively easy and cheaper alternative animal model for skin wound-healing studies. The entire full-thickness wound closure can be finished within 30–35 days. In zebrafish, faster re-epithelization occurred within 10 hrs after the skin was wounded, later followed up by inflammation/granulation tissue formation by 1–5 days postwound (dpw). By 6–9 dpw, scar resolution took place, and finally the skin wound fully recovered within 30 dpw [1,11,28]. Consistent with the previous study, in this experiment, zebrafish wounded with the laser engraving machine could close the wound at around 30–35 days (Figure 2B). In addition, compared to the previous literature, in this experiment, we defined 25% (12 dpw), 50% (16 dpw), and 75% (24 dpw) wound closure as three important endpoints to evaluate the wound healing-promoting potential to check the early, middle, and late stages of the wound-healing process in zebrafish. Interesting results could be obtained for skin wound healing in examples of astaxanthin and vitamin C. By 25% wound closure, vitamin C at a 2 ppm dose displayed more superior wound healing-promoting potential than astaxanthin. However, by 75% wound closure, astaxanthin at both 2 ppm and 20 ppm doses displayed more superior wound healing-promoting potential than vitamin C. This result suggests both antioxidants of astaxanthin and vitamin C indeed can boost wound closure in zebrafish, but with different potential. While astaxanthin has a better wound closure-promoting function than vitamin C during the late-wound-healing process, vitamin C has a better wound closure-promoting function than astaxanthin in the early-wound-healing process. Therefore, we strongly suggest this multiple-endpoint-based method should be applied to assess skin wound healing in zebrafish in order to obtain better resolution than the single-endpoint-based method that was performed in most previous studies [1,11,28]. In addition, this fast turn-around time makes it an ideal vertebrate model to conduct large-scale full-thickness wound-healing experiments. Since the zebrafish genome has been decoded, genetic manipulation tools, like transgenesis and genome editing, and chemical screening methods are also well established, paving the way to the creation of some transgenic or KO fish lines to overexpress or knockout some interesting candidates, discovered by transcriptomic data mining, to determine which among its gene functions plays an important role in full-thickness skin wound healing in the future.

4.3. Functional Validation of Ambient Temperature on Skin Wound Healing in Zebrafish

To check the consistency of the new method, several known factors and compounds for wound healing were tested. For the first experiment, wounded fish were exposed to different temperatures at 15°, 25° (control), and 35 °C. According to the results discovered in this study, a low temperature significantly delays the wound-healing process and a high temperature boosts the wound-healing process (Figure 7). In the low-temperature group of 15 °C, the 50% wound-closure time was almost three times slower when compared to the control group of 25 °C. The slow wound closure at lower temperatures might be due to immunosuppression, since previous studies showed that low temperatures will reduce neutrophils, fibroblasts, and epithelial cell activities and impair wound healing [86]. Furthermore, at low temperatures, fish such as Atlantic salmon are more vulnerable to skin lesions and infection by pathogens [87,88]. Another phenomenon in wound healing, like red mark syndrome (a nonlethal inflammatory skin disorder), also happens to rainbow trout at low temperatures [89,90]. Meanwhile, for higher temperatures, the result shows that the wound-healing process seems to be faster compared to the low-temperature and control groups (Figure 7). Our results are similar to other studies showing wound healing

in Atlantic salmon, cloud minnow, and European sea bass was significantly faster at higher-temperature conditions [17,91]. A recent experiment on Atlantic salmon (*Salmo solar* L.) that was held at two different temperatures (4 °C and 12 °C) also showed similar results as our experiment. According to the histology result, they found that Atlantic salmon held at a higher temperature (12 °C) indeed showed a faster wound-healing process [15]. According to these results, we strongly recommended the ambient temperature should be well controlled and reported when performing skin wound-healing experiments in zebrafish, since the overall skin wound closure was displayed in a strong temperature-dependent manner. Furthermore, based on these results, we confirmed that our method showed a consistent result for wound healing, as the results are in line with the prior study.

4.4. Functional Validation of Antioxidants on Promoting Skin Wound Healing in Zebrafish

Other than temperature, another factor, oxidative stress, was examined to perform more validation of this protocol. Antioxidants are known for their properties to enhance the healing of wounds by reducing the damage caused by oxygen radicals. Following the injuries, wounds are exposed to activated oxygen species released by infiltrating leukocytes. These reactive oxygen species (ROS) are usually generated by cells in response to the aerobic metabolism and the respiratory burst of phagocytic cells produced in response to pathogenic bacteria that invade the wounds [92,93]. ROS are produced in high amounts at the site of a wound as a defense mechanism against invading bacteria [92–94]; however, the high concentration of oxygen radicals induces severe tissue damage and leads to a delay in the healing process [95,96]. Antioxidants become the main defense and protection against ROS [97–99]. Antioxidants work by removing the products of inflammation, protecting the protease inhibitors from oxidative damage, and reducing the severe effect by inhibiting the residue of proteases and ROS that are formed by neutrophil accumulation at the wound site [100]. In this study, we validated two antioxidants, astaxanthin and vitamin C, and found that they could indeed boost the skin wound-healing process in zebrafish, which might be contributed to by ROS scavenging.

Astaxanthin is a natural xanthophyll carotenoid that can be found mostly in marine organisms [101,102]. Its antioxidative effect has been proven to be superior even to those of provitamins like vitamin A and vitamin E [103], and it is believed to be a potent antioxidant and one of the most powerful antioxidants. Meanwhile, vitamin C is an acidic, water-soluble antioxidant and a cofactor for collagen synthesis, which cannot be synthesized by humans due to L-gulonolactone oxidase (GLO) deficiency [104]. The wound-healing process requires a variety of macronutrients and micronutrients during each stage of healing to work properly [105,106]. Vitamin C is one of the required nutrients for wound healing during the proliferation phase, since, in this phase, fibroblasts produce collagen fibers which are related to and dependent upon vitamin C availability [107,108]. By utilizing the established method reported in this study, we were able to systematically compare the skin wound closure-promoting effect of those two compounds in zebrafish. According to the endpoints set at either the 25%, 50%, or 75% wound-closure percentage, we concluded that astaxanthin displayed more consistent and similar results with the previous experiment in mice, showing that topical treatment with an astaxanthin extract could accelerate wound healing in full-thickness dermal wounds [62]. Another study in cells suggested that the capability of astaxanthin in enhancing the wound-healing process was due to its ability to remove ROS and promote the wound-healing process by NIH 3T3 cells more effectively without causing cytotoxicity [37]. In the same manner, our study is also in line with a previous study in mice that demonstrated the way that vitamin C positively affects the early resolution of inflammation and tissue remodeling [109]. Furthermore, in another study of mice that were unable to synthesize vitamin C, vitamin C was provided in their water and the wound-healing process of the treated mice was checked. Later, they found that vitamin C could play an important role in wound healing by playing a crucial role in orchestrating multiple wound-healing processes [109]. Furthermore, similar results were also shown in another experiment on diabetic mice, which was orally administered with a

high dose of vitamin C to the mice and that successfully accelerated the wound-healing progress by increasing the angiogenesis [110]. In addition, other studies also found that the faster rate of wound closure by vitamin C in the early days was due to the properties that enable it to work on the collagen metabolism, which is crucial in the proliferation stage [107,109]. Interestingly, while a prior study has evaluated an adjuvant system and demonstrated a few clinical benefits in the nonsurgical treatment of peri-implant diseases, it showed no significant improvement in the present study [111]. Nevertheless, all of the results proved that the laser engraving machine and the protocol used in this study are indeed consistent, repeatable, and work properly as an alternative for wound-healing investigation. The development of this method also unlocks a limitless potency for us to perform a deeper investigation regarding the wound-healing process in fish, such as evaluating the effects of some adjuvant treatments, such as ozonized gel, that has been used for a periodontal patient [112], ozonized water, that has been tested to treat gingivitis patients and has been proven to be effective to reduce a microbial colony count [113], and probiotics, to investigate their mutual or synergize effect and their possible interaction.

4.5. Automatic Wound-Size Measurement by Using a Deep-Learning Approach

Previously published methods to measure the wound area in fish skin are largely relayed by ImageJ-based methods (summarized in Table A1). ImageJ was developed by NIH as an open-source software that is able to perform image analysis for biologists without coding training [114]. Using ImageJ software, users can manually mark the wound area and, later, conduct wound-size measurements by using the software's built-in function. However, this manual operation process is relatively tedious, time-consuming, and prone to operation mistakes. In order to overcome this shortage, in this study, we tested two deep learning-based tools, which were Mask RCNN and U-Net, on measuring the skin wound areas in zebrafish for the first time. Mask R-CNN and U-Net are both popular deep-learning architectures used for various computer vision tasks, including medical image segmentation, like skin lesion prediction [115–117]. The reason for testing two different methods is due to the different performances of Mask RCNN and U-Net on subject segmentation and recognition. For example, in humans, both methods have been used to measure skin lesions, and the result showed the Mask RCNN displayed superior performance than the U-Net [117]. In our previous works, we found that the U-Net performed better than the Mask RCNN on cardiac chamber size prediction for water fleas [118]. In this paper, we concluded that the U-Net displayed more superior performance than the Mask RCNN on skin wound-size prediction in zebrafish based on the evaluation of multiple parameters, like the Dice coefficient, IOU sensitivity, and specificity (Table 1). In general, the U-Net is particularly well-suited for cases where the object of interest (in this case, the skin wound) is smaller and more irregular in shape [95,96]. The other possible reason for the different performance between the Mask RCNN and U-Net is attributed to several factors: (1) Image datasets: the performance of any deep-learning model is significantly influenced by the quality and quantity of the datasets used for training and evaluation. Different papers employing diverse datasets or variations in datasets might result in variations in the overall performance of the constructed system. The diversity of the data, the presence of various types of skin lesions, and the quality of annotations all contribute to the model's ability to generalize. (2) Architecture of neural network: the Mask R-CNN and U-Net demonstrate distinct design approaches. The Mask R-CNN presents a more intricate structure amalgamating object detection and instance segmentation capabilities, enabling the anticipation of object masks and the categorization of instances contained within these masks. Conversely, the U-Net adopts a more streamlined architecture tailored for image segmentation. The efficacy of either architecture can vary based on the intricacies of the problem at hand and the subtleties inherent in the datasets. (3) Hyperparameter configuration: hyperparameters, such as the learning rate, batch size, and optimization algorithms, play a pivotal role in shaping the training procedure and model convergence. Divergent sets of hyperparameters across various studies can yield disparate training results and ultimate model performance.

It is imperative to acknowledge the absence of a universal solution in machine learning, and the selection among distinct architectures should hinge upon the unique problem context and accessible resources.

Another noteworthy discovery pertains to the applicability of the trained deep-learning model in predicting skin wound dimensions in other zebrafish strains exhibiting analogous stripe patterns. Both the Mask RCNN and U-Net methodologies exhibited comparable predictive efficacy for skin wound size in the TL and PET strains, which possess similar stripe patterns. In contrast, these deep-learning techniques demonstrated relatively diminished predictive accuracy when applied to skin wounds in the golden strain, characterized by fewer stripe patterns. This outcome underscores the pivotal role of skin stripe patterns in the training and learning procedures of both deep-learning methodologies. It is also worth noting that, although the currently established U-Net approach demonstrated a high success rate in predicting skin wound size in zebrafish, it exhibited a reduced predictive power and a heightened error rate when dealing with smaller wound areas (Figure 6). Therefore, we suggested that, to overcome this limitation, it might involve augmenting the training dataset with images depicting smaller wound sizes or adopting a hybrid two-phase model combining the Mask RCNN and U-Net [116,119].

Overall, the present study successfully developed a novel method for skin ablation and wound measurement in zebrafish. Here, the skin ablation process was programmed by the software, increasing the consistency of the wound area. However, this study still has some limitations, especially in the deep-learning wound measurement, although this only occurred for a relatively small wound size, since smaller wound areas are hard to distinguish. To overcome this issue and obtain optimal results, the contrast between the background and wound area needs to be clearer, and thus easy to be distinguished by the AI. Nevertheless, although the deep-learning measurement still has some limitations, it still provides much aid in calculating a lot of images, since, if it is performed manually, it could cause a lot of problems, such as subjectivity and human errors. In addition, this deep-learning measurement could also reduce the time needed to analyze the data. Finally, it is intriguing to explore the potencies of the current method in the future to examine potential medicines for wound healing.

5. Conclusions

Wound healing is an important process for organisms, and the enhancement of this process will benefit humans. To achieve this enhancement purpose, the improvement in the methodology to examine the process is necessary. This study successfully built a new method and protocol for wound healing that could create consistent and reliable results for skin wound-healing studies in zebrafish. The present method showed that it could produce a wound on zebrafish skin with consistency (2–3 mm). Moreover, the results in the temperature and antioxidant experiments showed that we could reproduce and repeat the data from prior studies. Higher temperature (35 °C) only needed ~6 days to close 25% of the wound, and only took ~12 days to reach 50% of wound closure, which was significantly faster compared to the control. Astaxanthin as an antioxidant also showed that it only needed ~7 days to close 25% of the wound and took ~12 days to reach 50% of wound closure. These results proved that our method works properly in zebrafish and can be used as an alternative to investigate any potential medicine for wound healing.

Furthermore, to boost the data calculation efficiency, deep learning-based methods were also adapted. By using the U-Net-based deep-learning method, the skin wound-size analysis can be conducted in a fully automatic manner for the first time in zebrafish. The utility of the trained U-Net model passed two rounds of validation for either temperature changes or antioxidant administration by showing a high sensitivity and specificity (± 0.8 and ~ 0.9 , respectively), although it could still be enhanced more in the future. Taken together, our studies demonstrated the laser-based instrument and trained deep-learning U-Net model reported here can offer scientists a standardized, convenient, and highly efficient method to address skin wound healing-relevant questions in zebrafish.

Author Contributions: Y.-K.L., C.-D.H. and H.-Y.L. participated in the study design. P.S., Y.-S.L., F.P.C., C.-Y.H., K.H.-C.C., J.-C.H. and C.-H.H. performed data curation and formal analysis. C.-D.H. provided funding acquisition and project administration. P.S., Y.-K.L., C.-D.H. and H.-Y.L. wrote the original draft. All authors have read and agreed to the published version of the manuscript.

Funding: This study was funded by grants sponsored by the Ministry of Science and Technology MOST 108-2313-B-033-001-MY3 to C.-D.H., E-Da Hospital and Southern Science Park Biotechnology and Medicine Industry Settlement Promotion Plan (DX-01-12-14-110), and E-Da Hospital (EDAHP110043/EDAHP111026) to Y.-S. Liu., and E-Da Cancer Hospital (EDCHP111006) to H.-Y. Lin.

Data Availability Statement: The data that support the findings of this study are available on request from the corresponding authors.

Acknowledgments: All authors reviewed the manuscript. We appreciate the anonymous reviewers and editors for their professional comments, which improved the quality of this paper. We also appreciate Gilbert Audira on helping paper editing.

Conflicts of Interest: The authors declare that they have no known competing financial interests or personal relationships that could have appeared to influence the work reported in this paper.

Appendix A

Table A1. Summary of some methods used from the previous experiment in wound healing in different fish models. The method established in our lab is highlighted in the first row.

Animal Model	Method to Induce Skin Wounds	Wound Size	Method to Measure Wound Size	Limitation	Author
Zebrafish	Laser ablation by using a laser engraving machine	2 mm in diameter	ImageJ and deep learning (Mask RCNN and U-Net)	AI methods still have some limitations in recognizing a smaller wound.	This study
Zebrafish	Razorblade; treatment with silver nanoparticles	Amputated the dorsal fin (fin loss)	Image by microscope and measured by ImageJ	ImageJ calculations are quite tedious and subjective, so mistakes in area measurement could occur, especially if the images are not clear.	Pang et al., 2020 [31]
Zebrafish	A laser beam from the dermal laser; treatment with silver nanoparticles	± 4 mm in diameter	Stereo microscope and measured by ImageJ	Measurements using ImageJ are subjective and tedious, so there will be some discrepancies between the measurements.	Seo et al., 2017 [32]
Zebrafish	A laser beam from the clinical dermal laser	2 mm in diameter	Manual measurement of wound size	Manual measurements are tedious and the subjectivity of the measurer could become a huge problem.	Richardson et al., 2013 [11]

Table A1. Cont.

Animal Model	Method to Induce Skin Wounds	Wound Size	Method to Measure Wound Size	Limitation	Author
Atlantic salmon	Biopsy punch at the abdomen	5 mm in diameter (scale loss)	Microscopy and measurement using Aperio ImageScope	Image quality could affect the result and complex steps for detection.	Sveen et al., 2019 [14]
<i>Cyprinus carpio</i>	Removal of the mucus using tissue paper, tissue swabs, and sandbag	15 mm in diameter	Histopathology and microscopy analysis	Histopathology is time-consuming and is limited by methodologic drawbacks.	Raj et al., 2011 [19]
Nile tilapia (<i>Oreochromis niloticus</i>)	Scalpel to induce an incision (cutting) wound at the dorsal musculature	Incisional (1 cm) (cut injury)	Histopathology	Histopathology is time-consuming and is limited by methodologic drawbacks.	Eissa et al., 2013 [120]
Gilthead seabream (<i>Sparus aurata</i> L.)	Circular biopsy punch (Stickel) below the lateral line	Diameter of 8 mm and depth of 2 mm	Image analysis software called Image-Pro Plus	Image quality can affect the final result, and can be computationally extensive, which limits the speed and efficiency.	Chen et al., 2020 [121]

References

- Richardson, R.J. Parallels between vertebrate cardiac and cutaneous wound healing and regeneration. *NPJ Regen. Med.* **2018**, *3*, 21. [\[CrossRef\]](#)
- Theoret, C. Tissue engineering in wound repair: The three “R” s—Repair, replace, regenerate. *Vet. Surg.* **2009**, *38*, 905–913. [\[CrossRef\]](#)
- Clark, R. Wound repair. Overview and general considerations. In *The Molecular and Cellular Biology of Wound Repair*; Springer Science: New York, NY, USA, 1994.
- Kawasumi, A.; Sagawa, N.; Hayashi, S.; Yokoyama, H.; Tamura, K. Wound healing in mammals and amphibians: Toward limb regeneration in mammals. In *New Perspectives in Regeneration*; Springer Science: New York, NY, USA, 2012; pp. 33–49.
- Masson-Meyers, D.S.; Andrade, T.A.; Caetano, G.F.; Guimaraes, F.R.; Leite, M.N.; Leite, S.N.; Frade, M.A.C. Experimental models and methods for cutaneous wound healing assessment. *Int. J. Exp. Pathol.* **2020**, *101*, 21–37. [\[CrossRef\]](#)
- Vandamme, T.F. Use of rodents as models of human diseases. *J. Pharm. Bioallied Sci.* **2014**, *6*, 2. [\[CrossRef\]](#) [\[PubMed\]](#)
- Smith, A.J.; Lilley, E.J.A. The role of the three Rs in improving the planning and reproducibility of animal experiments. *Animals* **2019**, *9*, 975. [\[CrossRef\]](#) [\[PubMed\]](#)
- Díaz, L.; Zambrano, E.; Flores, M.E.; Contreras, M.; Crispín, J.C.; Alemán, G.; Bravo, C.; Armenta-Espinosa, A.; Valdés, V.J.; Tovar, A.; et al. Ethical considerations in animal research: The principle of 3R’s. *Rev. Investig. Clin.* **2021**, *73*, 199–209. [\[CrossRef\]](#) [\[PubMed\]](#)
- Franco, N.H.; Olsson, I.A.S. Scientists and the 3Rs: Attitudes to animal use in biomedical research and the effect of mandatory training in laboratory animal science. *Lab. Anim.* **2014**, *48*, 50–60. [\[CrossRef\]](#)
- Kousholt, B.S.; Præstegaard, K.F.; Stone, J.C.; Thomsen, A.F.; Johansen, T.T.; Ritskes-Hoitinga, M.; Wegener, G. Reporting of 3Rs Approaches in Preclinical Animal Experimental Studies—A Nationwide Study. *Animals* **2023**, *13*, 3005. [\[CrossRef\]](#)
- Richardson, R.; Slanchev, K.; Kraus, C.; Knyphausen, P.; Eming, S.; Hammerschmidt, M. Adult zebrafish as a model system for cutaneous wound-healing research. *J. Investig. Dermatol.* **2013**, *133*, 1655–1665. [\[CrossRef\]](#)
- Guerra, R.; Santos, N.; Cecarelli, P.; Silva, J.; Hernandez-Blazquez, F. Healing of skin wounds in the African catfish *Clarias gariepinus*. *J. Fish Biol.* **2008**, *73*, 572–583. [\[CrossRef\]](#)
- Schmidt, J.G. Wound healing in rainbow trout (*Oncorhynchus mykiss*) and common carp (*Cyprinus carpio*): With a focus on gene expression and wound imaging. Ph.D. Thesis, Technical University of Denmark, Kongens Lyngby, Denmark, 2013.
- Sveen, L.R.; Timmerhaus, G.; Krasnov, A.; Takle, H.; Handeland, S.; Ytteborg, E. Wound healing in post-smolt Atlantic salmon (*Salmo salar* L.). *Sci. Rep.* **2019**, *9*, 3565. [\[CrossRef\]](#) [\[PubMed\]](#)
- Jensen, L.B.; Wahli, T.; McGurk, C.; Eriksen, T.B.; Obach, A.; Waagbø, R.; Handler, A.; Tafalla, C. Effect of temperature and diet on wound healing in Atlantic salmon (*Salmo salar* L.). *Fish Physiol. Biochem.* **2015**, *41*, 1527–1543. [\[CrossRef\]](#) [\[PubMed\]](#)

16. Roubal, F.; Bullock, A. The mechanism of wound repair in the skin of juvenile Atlantic salmon, *Salmo salar* L., following hydrocortisone implantation. *J. Fish Biol.* **1988**, *32*, 545–555. [\[CrossRef\]](#)
17. Anderson, C.; Roberts, R. A comparison of the effects of temperature on wound healing in a tropical and a temperate teleost. *J. Fish Biol.* **1975**, *7*, 173–182. [\[CrossRef\]](#)
18. Derwin, R.; Patton, D.; Avsar, P.; Strapp, H.; Moore, Z. The impact of topical agents and dressing on pH and temperature on wound healing: A systematic, narrative review. *Int. Wound J.* **2022**, *19*, 1397–1408. [\[CrossRef\]](#)
19. Raj, V.S.; Fournier, G.; Rakus, K.; Ronsmans, M.; Ouyang, P.; Michel, B.; Delforges, C.; Costes, B.; Farnir, F.; Leroy, B. Skin mucus of *Cyprinus carpio* inhibits cyprinid herpesvirus 3 binding to epidermal cells. *Vet. Res.* **2011**, *42*, 92. [\[CrossRef\]](#)
20. Sveen, L.R. Aquaculture Relevant Stressors and Their Impacts on Skin and Wound Healing in Post-Smolt Atlantic Salmon (*Salmo salar* L.). Doctoral Thesis, The University of Bergen, Bergen, Norway, 2018. Available online: <https://bora.uib.no/bora-xmloi/handle/1956/19024> (accessed on 21 February 2024).
21. Sveen, L.; Karlsen, C.; Ytteborg, E. Mechanical induced wounds in fish—a review on models and healing mechanisms. *Rev. Aquac.* **2020**, *12*, 2446–2465. [\[CrossRef\]](#)
22. Zordan, M.D.; Mill, C.P.; Riese, D.J.; Leary, J.F. A high throughput, interactive imaging, bright-field wound healing assay. *Cytom. Part A* **2011**, *79*, 227–232. [\[CrossRef\]](#)
23. Serena, T.E.; Cole, W.; Coe, S.; Harrell, K.; Serena, L.; Yaakov, R.; Rennie, M.Y. The safety of punch biopsies on hard-to-heal wounds: A large multicentre clinical trial. *J. Wound Care* **2020**, *29*, S4–S7. [\[CrossRef\]](#)
24. Jiang, Z.; Chen, J.; Wang, J.; Mangalindan, R.; Zhu, L.; Ladiges, W.C. A model for studying cutaneous wound healing and resilience to aging: Ear punch biopsy in old mice. *Aging Pathobiol. Ther.* **2020**, *2*, 173. [\[CrossRef\]](#)
25. Robinson, H.; Jarrett, P.; Vedhara, K.; Tarlton, J.; Whiting, C.; Law, M.; Broadbent, E. The effect of expressive writing on wound healing: Immunohistochemistry analysis of skin tissue two weeks after punch biopsy wounding. *J. Psychosom. Res.* **2022**, *161*, 110987. [\[CrossRef\]](#) [\[PubMed\]](#)
26. Feki, A.; Bardaa, S.; Hajji, S.; Ktari, N.; Hamdi, M.; Chabchoub, N.; Kallel, R.; Boudawara, T.; Nasri, M.; Amara, I.B. Falkenbergia rufolanosa polysaccharide–Poly (vinyl alcohol) composite films: A promising wound healing agent against dermal laser burns in rats. *Int. J. Biol. Macromol.* **2020**, *144*, 954–966. [\[CrossRef\]](#) [\[PubMed\]](#)
27. Capon, A.; Mordon, S. Can thermal lasers promote skin wound healing? *Am. J. Clin. Dermatol.* **2003**, *4*, 1–12. [\[CrossRef\]](#) [\[PubMed\]](#)
28. Richardson, R.; Metzger, M.; Knyphausen, P.; Ramezani, T.; Slanchev, K.; Kraus, C.; Schmelzer, E.; Hammerschmidt, M. Re-epithelialization of cutaneous wounds in adult zebrafish combines mechanisms of wound closure in embryonic and adult mammals. *Development* **2016**, *143*, 2077–2088. [\[CrossRef\]](#) [\[PubMed\]](#)
29. Shao, K.; Han, B.; Gao, J.; Jiang, Z.; Liu, W.; Liu, W.; Liang, Y. Fabrication and feasibility study of an absorbable diacetyl chitin surgical suture for wound healing. *J. Biomed. Mater. Res. Part B Appl. Biomater.* **2016**, *104*, 116–125. [\[CrossRef\]](#) [\[PubMed\]](#)
30. Khalkhal, E.; Razzaghi, M.; Rostami-Nejad, M.; Rezaei-Tavirani, M.; Beigvand, H.H.; Tavirani, M. Evaluation of laser effects on the human body after laser therapy. *J. Lasers Med. Sci.* **2020**, *11*, 91. [\[CrossRef\]](#) [\[PubMed\]](#)
31. Pang, S.; Gao, Y.; Wang, F.; Wang, Y.; Cao, M.; Zhang, W.; Liang, Y.; Song, M.; Jiang, G. Toxicity of silver nanoparticles on wound healing: A case study of zebrafish fin regeneration model. *Sci. Total Environ.* **2020**, *717*, 137178. [\[CrossRef\]](#)
32. Seo, S.B.; Dananjaya, S.; Nikapitiya, C.; Park, B.K.; Gooneratne, R.; Kim, T.-Y.; Lee, J.; Kim, C.-H.; De Zoysa, M. Silver nanoparticles enhance wound healing in zebrafish (*Danio rerio*). *Fish Shellfish Immunol.* **2017**, *68*, 536–545. [\[CrossRef\]](#)
33. Avdesh, A.; Chen, M.; Martin-Iverson, M.T.; Mondal, A.; Ong, D.; Rainey-Smith, S.; Taddei, K.; Lardelli, M.; Groth, D.M.; Verdile, G. Regular care and maintenance of a zebrafish (*Danio rerio*) laboratory: An introduction. *JoVE (J. Vis. Exp.)* **2012**, *69*, e4196.
34. Lopez-Luna, J.; Al-Jubouri, Q.; Al-Nuaimy, W.; Sneddon, L.U. Reduction in activity by noxious chemical stimulation is ameliorated by immersion in analgesic drugs in zebrafish. *J. Exp. Biol.* **2017**, *220*, 1451–1458. [\[CrossRef\]](#) [\[PubMed\]](#)
35. Collins, T.J. ImageJ for microscopy. *Biotechniques* **2007**, *43*, S25–S30. [\[CrossRef\]](#)
36. Mizuta, M.; Hirano, S.; Hiwatashi, N.; Tateya, I.; Kanemaru, S.; Nakamura, T.; Ito, J. Effect of astaxanthin on vocal fold wound healing. *Laryngoscope* **2014**, *124*, E1–E7. [\[CrossRef\]](#)
37. Oh, H.; Lee, J.S.; Sung, D.; Lim, J.-M.; Choi, W.I.J.I.o.N. Potential antioxidant and wound healing effect of nano-liposomal with high loading amount of astaxanthin. *Int. J. Nanomed.* **2020**, *15*, 9231–9240. [\[CrossRef\]](#)
38. Pérez-Escudero, A.; Vicente-Page, J.; Hinz, R.C.; Arganda, S.; De Polavieja, G.G. idTracker: Tracking individuals in a group by automatic identification of unmarked animals. *Nat. Methods* **2014**, *11*, 743. [\[CrossRef\]](#)
39. Audira, G.; Sampurna, B.P.; Juniardi, S.; Liang, S.-T.; Lai, Y.-H.; Hsiao, C.-D. A simple setup to perform 3D locomotion tracking in zebrafish by using a single camera. *Inventions* **2018**, *3*, 11. [\[CrossRef\]](#)
40. Eguiraun, H.; López-de-Ipiña, K.; Martinez, I. Application of entropy and fractal dimension analyses to the pattern recognition of contaminated fish responses in aquaculture. *Entropy* **2014**, *16*, 6133–6151. [\[CrossRef\]](#)
41. Nimkerdphol, K.; Nakagawa, M. Effect of sodium hypochlorite on zebrafish swimming behavior estimated by fractal dimension analysis. *J. Biosci. Bioeng.* **2008**, *105*, 486–492. [\[CrossRef\]](#) [\[PubMed\]](#)
42. Deakin, A.G.; Spencer, J.W.; Cossins, A.R.; Young, I.S.; Sneddon, L.U. Welfare challenges influence the complexity of movement: Fractal analysis of behaviour in zebrafish. *Fishes* **2019**, *4*, 8. [\[CrossRef\]](#)
43. Tokuda, K.; Baron, B.; Kuramitsu, Y.; Kitagawa, T.; Tokuda, N.; Morishige, N.; Kobayashi, M.; Kimura, K.; Nakamura, K.; Sonoda, K.H. Optimization of fixative solution for retinal morphology: A comparison with Davidson’s fixative and other fixation solutions. *Jpn. J. Ophthalmol.* **2018**, *62*, 481–490. [\[CrossRef\]](#)

44. Sneddon, L.U.; Elwood, R.W.; Adamo, S.A.; Leach, M.C. Defining and assessing animal pain. *Anim. Behav.* **2014**, *97*, 201–212. [[CrossRef](#)]
45. Sneddon, L.U. Evolution of nociception and pain: Evidence from fish models. *Philos. Trans. R. Soc. B* **2019**, *374*, 20190290. [[CrossRef](#)] [[PubMed](#)]
46. Kalueff, A.V.; Kaluyeva, A.; Maillet, E.L. Anxiolytic-like effects of noribogaine in zebrafish. *Behav. Brain Res.* **2017**, *330*, 63–67. [[CrossRef](#)] [[PubMed](#)]
47. Li, F.; Wang, C.; Liu, X.; Peng, Y.; Jin, S. A composite model of wound segmentation based on traditional methods and deep neural networks. *Comput. Intell. Neurosci.* **2018**, *2018*, 4149103. [[CrossRef](#)] [[PubMed](#)]
48. Carrión, H.; Jafari, M.; Bagoood, M.D.; Yang, H.-Y.; Isseroff, R.R.; Gomez, M. Automatic wound detection and size estimation using deep learning algorithms. *PLoS Comput. Biol.* **2022**, *18*, e1009852. [[CrossRef](#)]
49. Shorten, C.; Khoshgoftaar, T.M. A survey on image data augmentation for deep learning. *J. Big Data* **2019**, *6*, 1–48. [[CrossRef](#)]
50. Frid-Adar, M.; Klang, E.; Amitai, M.; Goldberger, J.; Greenspan, H. Synthetic data augmentation using GAN for improved liver lesion classification. In Proceedings of the 2018 IEEE 15th International Symposium on Biomedical Imaging (ISBI 2018), Washington, DC, USA, 4–7 April 2018.
51. Buslaev, A.; Iglovikov, V.I.; Khvedchenya, E.; Parinov, A.; Druzhinin, M.; Kalinin, A.A. Albumentations: Fast and flexible image augmentations. *Information* **2020**, *11*, 125. [[CrossRef](#)]
52. Ronneberger, O.; Fischer, P.; Brox, T. U-net: Convolutional networks for biomedical image segmentation. In Proceedings of the International Conference on Medical Image Computing and Computer-Assisted Intervention, Munich, Germany, 5–9 October 2015; Springer: Berlin/Heidelberg, Germany, 2015.
53. Falk, T.; Mai, D.; Bensch, R.; Çiçek, Ö.; Abdulkadir, A.; Marrakchi, Y.; Böhm, A.; Deubner, J.; Jäckel, Z.; Seiwald, K. U-Net: Deep learning for cell counting, detection, and morphometry. *Nat. Methods* **2019**, *16*, 67–70. [[CrossRef](#)]
54. Kido, S.; Hirano, Y.; Hashimoto, N. Detection and classification of lung abnormalities by use of convolutional neural network (CNN) and regions with CNN features (R-CNN). In Proceedings of the 2018 International Workshop on Advanced Image Technology (IWAIT), Chiang Mai, Thailand, 7–9 January 2018.
55. Jadon, S. A survey of loss functions for semantic segmentation. In Proceedings of the 2020 IEEE Conference on Computational Intelligence in Bioinformatics and Computational Biology (CIBCB), Vina del Mar, Chile, 27–29 October 2020.
56. Finn, J.P.; Nielsen, N. The effect of temperature variation on the inflammatory response of rainbow trout. *J. Pathol.* **1971**, *105*, 257–268. [[CrossRef](#)] [[PubMed](#)]
57. Bullock, A.M.; Marks, R.; Roberts, R.J. The cell kinetics of teleost fish epidermis: Epidermal mitotic activity in relation to wound healing at varying temperatures in plaice (*Pleuronectes platessa*). *J. Zool.* **1978**, *185*, 197–204. [[CrossRef](#)]
58. Post, G. *The Immune Response of Rainbow Trout: (Salmo Gairdnerii) to Aeromonas Hydrophila*; Utah State Department of Fish and Game: Vernal, UT, USA, 1963.
59. Shanmugapriya, K.; Kim, H.; Saravana, P.S.; Chun, B.-S.; Kang, H.W. Astaxanthin-alpha tocopherol nanoemulsion formulation by emulsification methods: Investigation on anticancer, wound healing, and antibacterial effects. *Colloids Surf. B Biointerfaces* **2018**, *172*, 170–179. [[CrossRef](#)] [[PubMed](#)]
60. Bartlett, M.K.; Jones, C.M.; Ryan, A.E. Vitamin C and wound healing: II. Ascorbic acid content and tensile strength of healing wounds in human beings. *N. Engl. J. Med.* **1942**, *226*, 474–481. [[CrossRef](#)]
61. Lund, C.C.; Crandon, J.H. Ascorbic acid and human wound healing. *Ann. Surg.* **1941**, *114*, 776. [[CrossRef](#)]
62. Meephansan, J.; Rungjang, A.; Yingmema, W.; Deenonpoe, R.; Ponnikorn, S. Effect of astaxanthin on cutaneous wound healing. *Clin. Cosmet. Investig. Dermatol.* **2017**, *10*, 259. [[CrossRef](#)]
63. YUSOF, A.A. The effects of Carica papaya Linn. latex on the healing of burn wounds in rats. *J. Sains Kesihat. Malays.* **2005**, *3*, 39–47.
64. Jalalpure, S.S.; Agrawal, N.; Patil, M.; Chimkode, R.; Tripathi, A. Antimicrobial and wound healing activities of leaves of Alternanthera sessilis Linn. *Int. J. Green Pharm. (IJGP)* **2008**, *2*, 141. [[CrossRef](#)]
65. Jonkman, J.E.; Cathcart, J.A.; Xu, F.; Bartolini, M.E.; Amon, J.E.; Stevens, K.M.; Colarusso, P. An introduction to the wound healing assay using live-cell microscopy. *Cell Adhes. Migr.* **2014**, *8*, 440–451. [[CrossRef](#)]
66. Shaw, T.J.; Martin, P. Wound repair at a glance. *J. Cell Sci.* **2009**, *122*, 3209–3213. [[CrossRef](#)] [[PubMed](#)]
67. Zahm, J.M.; Kaplan, H.; Hérad, A.L.; Doriot, F.; Pierrot, D.; Somelette, P.; Puchelle, E. Cell migration and proliferation during the in vitro wound repair of the respiratory epithelium. *Cell Motil. Cytoskelet.* **1997**, *37*, 33–43. [[CrossRef](#)]
68. Coomber, B.L.; Gotlieb, A.I. In vitro endothelial wound repair. Interaction of cell migration and proliferation. *Arterioscler. Off. J. Am. Heart Assoc. Inc.* **1990**, *10*, 215–222. [[CrossRef](#)] [[PubMed](#)]
69. Yue, P.Y.; Leung, E.P.; Mak, N.; Wong, R.N. A simplified method for quantifying cell migration/wound healing in 96-well plates. *SLAS Discov. Adv. Sci. Drug Discov.* **2010**, *15*, 427–433. [[CrossRef](#)]
70. Dorsett-Martin, W.A. Rat models of skin wound healing: A review. *Wound Repair Regen.* **2004**, *12*, 591–599. [[CrossRef](#)]
71. Sullivan, T.P.; Eaglstein, W.H.; Davis, S.C.; Mertz, P. The pig as a model for human wound healing. *Wound Repair Regen.* **2001**, *9*, 66–76. [[CrossRef](#)]
72. Abergel, R.P.; Lyons, R.; Dwyer, R.; White, R.R.; Uitto, J. Use of lasers for closure of cutaneous wounds: Experience with Nd: YAG, argon and CO₂ lasers. *J. Dermatol. Surg. Oncol.* **1986**, *12*, 1181–1185. [[CrossRef](#)] [[PubMed](#)]
73. Spadoni, D.; Cain, C.L. Facial resurfacing. Using the carbon dioxide laser. *AORN J.* **1989**, *50*, 1009–1013. [[CrossRef](#)]

74. Romanos, G.E.; Pelekanos, S.; Strub, J.R. Effects of Nd: YAG laser on wound healing processes: Clinical and immunohistochemical findings in rat skin. *Lasers Surg. Med.* **1995**, *16*, 368–379. [\[CrossRef\]](#) [\[PubMed\]](#)
75. Posten, W.; Wrone, D.A.; Dover, J.S.; Arndt, K.A.; Silapunt, S.; Alam, M. Low-level laser therapy for wound healing: Mechanism and efficacy. *Dermatol. Surg.* **2005**, *31*, 334–340. [\[CrossRef\]](#) [\[PubMed\]](#)
76. Mester, E. The effect of laser radiation on wound healing and collagen synthesis. *Stimul. Newslett.* **1973**, 55–59. Available online: <https://inis.iaea.org/search/searchsinglerecord.aspx?recordsFor=SingleRecord&RN=4078961> (accessed on 18 February 2024).
77. Mester, E.; Spiry, T.; Szende, B.; Tota, J.G. Effect of laser rays on wound healing. *Am. J. Surg.* **1971**, *122*, 532–535. [\[CrossRef\]](#) [\[PubMed\]](#)
78. Kana, J.S.; Hutschenreiter, G. Effect of low—Power density laser radiation on healing of open skin wounds in rats. *Arch. Surg.* **1981**, *116*, 293–296. [\[CrossRef\]](#)
79. Dyson, M.; Young, S. Effect of laser therapy on wound contraction and cellularity in mice. *Lasers Med. Sci.* **1986**, *1*, 125–130. [\[CrossRef\]](#)
80. Carvalho, P.d.T.C.d.; Mazzer, N.; Reis, F.A.d.; Belchior, A.C.G.; Silva, I.S. Analysis of the influence of low-power HeNe laser on the healing of skin wounds in diabetic and non-diabetic rats. *Acta Cir. Bras.* **2006**, *21*, 177–183. [\[CrossRef\]](#)
81. Samaneh, R.; Ali, Y.; Mostafa, J.; Mahmud, N.A.; Zohre, R. Laser therapy for wound healing: A review of current techniques and mechanisms of action. *Biosci. Biotechnol. Res. Asia* **2015**, *12*, 217–223. [\[CrossRef\]](#)
82. Lemes, C.H.J.; da Rosa, W.L.d.O.; Sonego, C.L.; Lemes, B.J.; Moraes, R.R.; da Silva, A.F. Does laser therapy improve the wound healing process after tooth extraction? A systematic review. *Wound Repair Regen.* **2019**, *27*, 102–113. [\[CrossRef\]](#) [\[PubMed\]](#)
83. Grada, A.; Mervis, J.; Falanga, V. Research techniques made simple: Animal models of wound healing. *J. Investig. Dermatol.* **2018**, *138*, 2095–2105.e1. [\[CrossRef\]](#) [\[PubMed\]](#)
84. Lindblad, W.J. Considerations for selecting the correct animal model for dermal wound-healing studies. *J. Biomater. Sci. Polym. Ed.* **2008**, *19*, 1087–1096. [\[CrossRef\]](#)
85. Parnell, L.K.; Volk, S.W. The evolution of animal models in wound healing research: 1993–2017. *Adv. Wound Care* **2019**, *8*, 692–702. [\[CrossRef\]](#)
86. Xia, Z.; Sato, A.; Hughes, M.A.; Cherry, G.W. Stimulation of fibroblast growth in vitro by intermittent radiant warming. *Wound Repair Regen.* **2000**, *8*, 138–144. [\[CrossRef\]](#)
87. Benediktsdóttir, Helgason; Sigurjónsdóttir. *Vibrio* spp. isolated from salmonids with shallow skin lesions and reared at low temperature. *J. Fish Dis.* **1998**, *21*, 19–28.
88. Løvoll, M.; Wiik-Nielsen, C.; Tunsjø, H.S.; Colquhoun, D.; Lunder, T.; Sørsum, H.; Grove, S. Atlantic salmon bath challenged with *Moritella viscosa*—pathogen invasion and host response. *Fish Shellfish Immunol.* **2009**, *26*, 877–884. [\[CrossRef\]](#)
89. Metselaar, M.; Thompson, K.; Gratacap, R.; Kik, M.J.; LaPatra, S.E.; Lloyd, S.J.; Call, D.R.; Smith, P.; Adams, A. Association of red-mark syndrome with a Rickettsia-like organism and its connection with strawberry disease in the USA. *J. Fish Dis.* **2010**, *33*, 849–858. [\[CrossRef\]](#)
90. Verner-Jeffreys, D.; Pond, M.; Peeler, E.; Rimmer, G.; Oidtmann, B.; Way, K.; Mewett, J.; Jeffrey, K.; Bateman, K.; Reese, R. Emergence of cold water strawberry disease of rainbow trout *Oncorhynchus mykiss* in England and Wales: Outbreak investigations and transmission studies. *Dis. Aquat. Org.* **2008**, *79*, 207–218. [\[CrossRef\]](#)
91. Mateus, A.P.; Costa, R.A.; Sadoul, B.; Bégout, M.-L.; Cousin, X.; Canario, A.V.; Power, D.M. Thermal imprinting during embryogenesis modifies skin repair in juvenile European sea bass (*Dicentrarchus labrax*). *Fish Shellfish Immunol.* **2023**, *134*, 108647. [\[CrossRef\]](#)
92. Jamieson, D. Oxygen toxicity and reactive oxygen metabolites in mammals. *Free Radic. Biol. Med.* **1989**, *7*, 87–108. [\[CrossRef\]](#)
93. Janoff, A.; Carp, H. Proteases, antiproteases, and oxidants: Pathways of tissue injury during inflammation. *Monogr. Pathol.* **1982**, *23*, 62–82.
94. Reddy, B.S.; Reddy, R.K.K.; Naidu, V.; Madhusudhana, K.; Agwane, S.B.; Ramakrishna, S.; Diwan, P.V. Evaluation of antimicrobial, antioxidant and wound-healing potentials of *Holoptelea integrifolia*. *J. Ethnopharmacol.* **2008**, *115*, 249–256. [\[CrossRef\]](#)
95. Jorge, M.P.; Madjarof, C.; Ruiz, A.L.T.G.; Fernandes, A.T.; Rodrigues, R.A.F.; de Oliveira Sousa, I.M.; Foglio, M.A.; de Carvalho, J.E. Evaluation of wound healing properties of *Arrabidaea chica* Verlot extract. *J. Ethnopharmacol.* **2008**, *118*, 361–366. [\[CrossRef\]](#)
96. Dunnill, C.; Patton, T.; Brennan, J.; Barrett, J.; Dryden, M.; Cooke, J.; Leaper, D.; Georgopoulos, N.T. Reactive oxygen species (ROS) and wound healing: The functional role of ROS and emerging ROS-modulating technologies for augmentation of the healing process. *Int. Wound J.* **2017**, *14*, 89–96. [\[CrossRef\]](#) [\[PubMed\]](#)
97. Martin, A. The use of antioxidants in healing. *Dermatol. Surg.* **1996**, *22*, 156–160. [\[CrossRef\]](#) [\[PubMed\]](#)
98. Birben, E.; Sahiner, U.M.; Sackesen, C.; Erzurum, S.; Kalayci, O. Oxidative stress and antioxidant defense. *World Allergy Organ. J.* **2012**, *5*, 9–19. [\[CrossRef\]](#) [\[PubMed\]](#)
99. Dumanović, J.; Nepovimova, E.; Natić, M.; Kuča, K.; Jačević, V. The significance of reactive oxygen species and antioxidant defense system in plants: A concise overview. *Front. Plant Sci.* **2021**, *11*, 552969. [\[CrossRef\]](#) [\[PubMed\]](#)
100. Houghton, P.; Hylands, P.; Mensah, A.; Hensel, A.; Deters, A. In vitro tests and ethnopharmacological investigations: Wound healing as an example. *J. Ethnopharmacol.* **2005**, *100*, 100–107. [\[CrossRef\]](#) [\[PubMed\]](#)
101. Higuera-Ciapara, I.; Felix-Valenzuela, L.; Goycoolea, F. Astaxanthin: A review of its chemistry and applications. *Crit. Rev. Food Sci. Nutr.* **2006**, *46*, 185–196. [\[CrossRef\]](#)

102. Yaqoob, Z.; Arshad, M.S.; Imran, M.; Munir, H.; Qaisrani, T.B.; Khalid, W.; Asghar, Z.; Suleria, H.A.R. Mechanistic role of astaxanthin derived from shrimp against certain metabolic disorders. *Food Sci. Nutr.* **2022**, *10*, 12–20. [[CrossRef](#)] [[PubMed](#)]
103. Nishida, Y.; Yamashita, E.; Miki, W. Quenching activities of common hydrophilic and lipophilic antioxidants against singlet oxygen using chemiluminescence detection system. *Carotenoid Sci.* **2007**, *11*, 16–20.
104. Linster, C.L.; Van Schaftingen, E. Vitamin C: Biosynthesis, recycling and degradation in mammals. *FEBS J.* **2007**, *274*, 1–22. [[CrossRef](#)] [[PubMed](#)]
105. Lansdown, A.; Sampson, B.; Rowe, A. Sequential changes in trace metal, metallothionein and calmodulin concentrations in healing skin wounds. *J. Anat.* **1999**, *195*, 375–386. [[CrossRef](#)] [[PubMed](#)]
106. Patel, G.K. The role of nutrition in the management of lower extremity wounds. *Int. J. Low. Extrem. Wounds* **2005**, *4*, 12–22. [[CrossRef](#)] [[PubMed](#)]
107. Flanagan, M. *Wound Management*, 1st ed.; Churchill Livingstone: London, UK, 1997.
108. Moores, J. Vitamin C: A wound healing perspective. *Br. J. Community Nurs.* **2013**, *18*, S6–S11. [[CrossRef](#)] [[PubMed](#)]
109. Mohammed, B.M.; Fisher, B.J.; Kraskauskas, D.; Ward, S.; Wayne, J.S.; Brophy, D.F.; Fowler III, A.A.; Yager, D.R.; Natarajan, R. Vitamin C promotes wound healing through novel pleiotropic mechanisms. *Int. Wound J.* **2016**, *13*, 572–584. [[CrossRef](#)]
110. Chokesuwattanaskul, S.; Sukpat, S.; Duangpatra, J.; Buppajarntham, S.; Decharatanachart, P.; Mutirangura, A.; Patumraj, S. High dose oral vitamin C and mesenchymal stem cells aid wound healing in a diabetic mouse model. *J. Wound Care* **2018**, *27*, 334–339. [[CrossRef](#)]
111. Butera, A.; Maiorani, C.; Gallo, S.; Pascadopoli, M.; Venugopal, A.; Marya, A.; Scribante, A. Evaluation of adjuvant systems in non-surgical peri-implant treatment: A literature review. *Healthcare* **2022**, *10*, 886. [[CrossRef](#)]
112. Scribante, A.; Gallo, S.; Pascadopoli, M.; Frani, M.; Butera, A. Ozonized gels vs chlorhexidine in non-surgical periodontal treatment: A randomized clinical trial. In *Oral Diseases*; Wiley Online Library: Hoboken, NJ, USA, 2023.
113. Talasani, R.R.; Potharaju, S.P.; Lakshmi, B.V.; Bai, Y.D.; Chintala, R.K.; Mahankali, V.; AlGhamdi, A.R.S. Efficacy of ozonated water over chlorhexidine mouth rinse in chronic gingivitis patients—A comparative clinical study. *Saudi Dent. J.* **2022**, *34*, 738–743. [[CrossRef](#)] [[PubMed](#)]
114. Abràmoff, M.D.; Magalhães, P.J.; Ram, S.J. Image processing with ImageJ. *Biophotonics Int.* **2004**, *11*, 36–42.
115. Vuola, A.O.; Akram, S.U.; Kannala, J. Mask-RCNN and U-net ensemble for nuclei segmentation. In Proceedings of the 2019 IEEE 16th International Symposium on Biomedical Imaging (ISBI 2019), Venice, Italy, 8–11 April 2019.
116. Dogan, R.O.; Dogan, H.; Bayrak, C.; Kayikcioglu, T. A two-phase approach using mask R-CNN and 3D U-Net for high-accuracy automatic segmentation of pancreas in CT imaging. *Comput. Methods Programs Biomed.* **2021**, *207*, 106141. [[CrossRef](#)] [[PubMed](#)]
117. Alfaro, E.; Fonseca, X.B.; Albornoz, E.M.; Martínez, C.E.; Ramrez, S.C. A brief analysis of u-net and mask r-cnn for skin lesion segmentation. In Proceedings of the 2019 IEEE International Work Conference on Bioinspired Intelligence (IWOBI), Budapest, Hungary, 3–5 July 2019.
118. Saputra, F.; Farhan, A.; Suryanto, M.E.; Kurnia, K.A.; Chen, K.H.-C.; Vasquez, R.D.; Roldan, M.J.M.; Huang, J.-C.; Lin, Y.-K.; Hsiao, C.-D. Automated Cardiac Chamber Size and Cardiac Physiology Measurement in Water Fleas by U-Net and Mask RCNN Convolutional Networks. *Animals* **2022**, *12*, 1670. [[CrossRef](#)]
119. Widyaningrum, R.; Candradewi, I.; Aji, N.R.A.S.; Aulianisa, R. Comparison of Multi-Label U-Net and Mask R-CNN for panoramic radiograph segmentation to detect periodontitis. *Imaging Sci. Dent.* **2022**, *52*, 383. [[CrossRef](#)]
120. Eissa, A.; Zaki, M.; Saeid, S.; Abdelsalam, M.; Ali, H.; Moustafa, A.; Ibrahim, T.; Abumhara, A. In vitro evaluation of the efficacy of hemodialysate (Solcoseryl®) as a wound healing agent in Nile tilapia (*Oreochromis niloticus*). *Int. J. Vet. Sci. Med.* **2013**, *1*, 57–64. [[CrossRef](#)]
121. Chen, Z.; Ceballos-Francisco, D.; Guardiola, F.A.; Huang, D.; Esteban, M.Á. Skin wound healing in gilthead seabream (*Sparus aurata* L.) fed diets supplemented with arginine. *Fish Shellfish Immunol.* **2020**, *104*, 347–358. [[CrossRef](#)]

Disclaimer/Publisher’s Note: The statements, opinions and data contained in all publications are solely those of the individual author(s) and contributor(s) and not of MDPI and/or the editor(s). MDPI and/or the editor(s) disclaim responsibility for any injury to people or property resulting from any ideas, methods, instructions or products referred to in the content.